2016

SHEAR DRIVEN SUPPRESSED NUCLEATION ANNULAR FLOW-BOILING IN MILLIMETER-SCALE CHANNELS: DIRECT NUMERICAL SIMULATIONS

Sharayu Bhasme
Michigan Technological University, ssbhasme@mtu.edu

SHEAR DRIVEN SUPPRESSED NUCLEATION ANNULAR FLOW-BOILING IN MILLIMETER-SCALE CHANNELS: DIRECT NUMERICAL SIMULATIONS

By

Sharayu S. Bhasme

A THESIS

Submitted in partial fulfillment of the requirements for the degree of

MASTER OF SCIENCE

In Mechanical Engineering

MICHIGAN TECHNOLOGICAL UNIVERSITY

2016

This thesis has been approved in partial fulfillment of the requirements for the Degree of MASTER OF SCIENCE in Mechanical Engineering.

Department of Mechanical Engineering – Engineering Mechanics

Thesis Advisor: *Dr Amitabh Narain*

Committee Member: *Dr V. C Rao Komaravolu*

Committee Member: *Dr Sunil Mehendale*

Department Chair: *Dr William W Predebon*

Contents

List of Figures 4

List of Tables 5

Preface 6

Acknowledgments 7

List of Abbreviations 9

Abstract 11

1 Introduction 12

2. Problem Statement and Governing Equations 17

2.1. Interior Equations 20

2.2. Interface Conditions 22

2.3. Boundary Conditions for Combined Consideration of the Vapor and Liquid Domains 26

3. Computational Approach and Algorithm 31

4. Results and Discussions 37

4.1 Grid Size Restrictions 37

4.2 Basic Flow Features of Suppressed Nucleation Annular Boiling 42

5. Conclusions 49

6. Forthcoming Results 50

REFERENCES 51

APPENDICES 55

APPENDIX A1 55

APPENDIX A2 59

APPENDIX A3 67

List of Figures

Fig. 1.1: Innovative boiler's [1] non-pulsatile operation 12

Fig. 1.2: A schematic of a traditional flow-boiling operation in a channel with bottom wall heating..... 13

Fig. 2.1: (a) Schematic of a representative suppressed nucleation case of annular flow boiling in a channel. (b) Schematic of a representative instantaneous interface location showing the interfacial variables used as boundary conditions for the liquid and the vapor domains. The computational domain's exit at x = Lcomp in (b) is often slightly larger than the exit at x = L in (a) 18

Fig. 2.2 (a) Representative Wall temperature (Tw(x)) prescribed "methods of heating" over xp ≥ 0 & -xp* <xp<0. (b) Representative wall heat flux (q"w(x)) prescribed "methods of heating" over xp ≥ 0 & -xp* <xp<0..... 28

Fig. 2.3 Representative film thickness profile for "method of heating" in Fig 2.2 30

Fig. 4.1: The mesh comparison for: (a) a representative liquid domain solution and (b) a representative vapor domain solution. The "order of convergence" study, not reported here, yields results similar to what has been reported in [30, 38] (Run parameters: Fluid – FC72, U – 1 m/s, p0 = 105.1 kPa, ΔT = 10°C, h = 2 mm). 39

Fig. 4.2: (a) Plot of a steady film thickness profile for a horizontal case involving presence of transverse gravity. Cross-sectional profile plots at xp = 0.02 m are shown for: (b) x-component of velocity uI, (c) y-component of velocity vI, and (d) Temperature TI, and (e) pressure pI. The x-variation of 1-D flow variables: (f) $\overline{u}(x^p)$ and $u_1^i(x^p)$; (g) $\tau^{int}(x^p)$; (Run parameters: Fluid – FC-72, U = 1 m/s, p0 = 105.1 kPa, ΔT = 10°C, channel height = 2 mm, G ≡ ρ2U = 13.98 kg/m2s)..... 46

Fig. 4.3: The x-variation of 1-D heat transfer variables for the flow in Fig. 4.2: (a) $\dot{m}^p(x^p)$ (b) $q''_w(x)$ (Run case: same as in Fig 4.2.)..... 48

Fig. A2.1: Schematic of the adiabatic laminar/laminar flow zone corresponding to uniform liquid film thickness of Δ0..... 59

Fig. A2.2: Comparison of correlations with Zivi Correlation (Parameters: (ρ_2/ρ_1) = 0.0095, (μ_2/μ_1) = 0.024)..... 65

List of Tables

Table 4.1: Table shows representative mesh sizes for different meshes 40

Table 4.2: Table shows representative satisfaction of interface conditions for different locations along the length of the channel 41

Preface

This thesis is submitted in partial fulfillment of Degree of Master of Science in Mechanical Engineering at Michigan Technological University. The research reported here was carried out under the guidance of Dr Amitabh Narain. The research pertaining to code development for suppressed nucleate annular boiling flows starting with prior heating method (using flow condensation code developed by Dr Narain's research group) reported here was done by me. It wouldn't have been possible to shape this thesis without the invaluable help from my research team member, Hrishikesh Prasad who has worked on post – processing this code to generate correlations for suppressed nucleate annular boiling flows.

Acknowledgments

This thesis would not have been possible without the invaluable support and encouragement from many individuals in many ways and I would like to express my sincere thanks to all of them.

First and foremost I would like to thank my academic advisor, Dr Amitabh Narain for constantly guiding me throughout my research and imparting his immense knowledge in this field. Without his innovative ideas and supervision this endeavor wouldn't have been possible.

My heartfelt thanks to Dr Ranjeeth Naik for helping me implement the research ideas. His expertise in writing codes, using simulation tools and willing assistance certainly helped me a lot throughout the course of this research. The flow condensation code developed by him was used by me to develop the suppressed nucleate annular flow boiling code.

I am also thankful to my research team member, Hrishikesh Prasad for helping me write this thesis and for post-processing the annular flow boiling code developed by me to generate correlations. Without his help it would not have been possible to finish this thesis in time.

I would also like to thank Dr Sunil Mehendale and Dr V C Komaravalu for being a part of my defense committee and helping me complete this thesis successfully.

Many thanks to all my friends, particularly Ajinkya Rohankar for his immense emotional support and constant encouragement which helped me complete this work successfully in time.

Above all, I am grateful to my parents and my sister for all their love and support without which it wouldn't have been possible to achieve this.

List of Abbreviations

C_p	Specific Heat, J/kg-K
Fr_x	Froude Number in x-direction, $(U/(g_x h)^{1/2})$
Fr_y	Froude Number in y-direction, $(U/(g_y h)^{1/2})$
G	Mass-flux for steady annular boiling, kg/m^2s
g_x	Gravity component in x-direction, m/s^2
g_y	Gravity component in y-direction, m/s^2
h	Height of the channel, m
h_{fg}	Heat of vaporization, J/kg
Ja	Liquid Jakob Number $(C_{p1}\Delta T/h_{fg}(p_0))$
k	Conductivity, W/m-K
L	Length of the channel or test-section, m
$\dot{m}^p$	Local interfacial mass flux, kg/m^2-s
p_0	Steady inlet pressure (also p_{in}), kPa
Pr_1	Liquid Prandtl Number $(\mu_1 C_{p1}/k_1)$
$\overline{q}_w$	Mean wall heat flux, W/m^2
Re_{T-V}	Reynolds number representing non-dimensional G (Gh/μ_2)
$\overline{T}_w$	Mean Boiling surface temperature, °C
$T_{sat}(p_0)$	Saturation Temperature at pressure p_0, °C
u_I, v_I	Non-dimensional velocities in x and y-directions
U	Average inlet vapor velocity in the x-direction (obtained from $G = \rho_2 U$), m/s
w	Cross-sectional width of the channel, m
We	Liquid Weber Number $(\rho_1 U^2 h/\sigma)$
x, y	Non-dimensional distances along with and perpendicular to the boiling surface
x_A	Non-dimensional length of the annular regime

Greek Symbols

δ	Non-dimensional liquid film thickness
Δ	Physical value of liquid film thickness, m
θ	Non-dimensional temperature
μ	Viscosity, kg/m-s
ρ	Density, kg/m^3

Subscripts

1 or L	Represents liquid phase of the flow variable
2 or V	Represents vapor phase of the flow variable
e	Represents "entrance effect" due to heating conditions prior to inlet

Superscripts

p	Physical value of a variable, e.g. x^p – associated with non-dimensional x
i	Value of the flow variable at the interface

Abstract

Many contemporary high heat-flux cooling applications are facilitated by mm-scale flow-boilers that operate in the steady annular suppressed nucleation regime (i.e., a thin evaporating liquid film flow covers the heated boiling-surface).

For such cases, this thesis presents a direct numerical simulation (DNS) approach. The steady algorithm and its accuracy are discussed. Representative detailed solutions for annular flow-boiling of FC-72 in a horizontal channel are presented.

Keywords: Shear-driven annular flow-boiling, millimeter scale flow-boilers, steady annular evaporating flows, high heat-flux cooling.

1 Introduction

This thesis presents fundamental modeling and first-principles based computational results (including heat-transfer correlations) for suppressed nucleation cases of shear/pressure driven annular flow boiling in horizontal millimeter-scale channels (or rectangular cross-section ducts of large aspect-ratio). Both temperature and heat flux controlled heating of the bottom horizontal plate – important for innovative flow boiling operations (see Fig. 1.1 below and [1]) – is considered in the proposed algorithm.

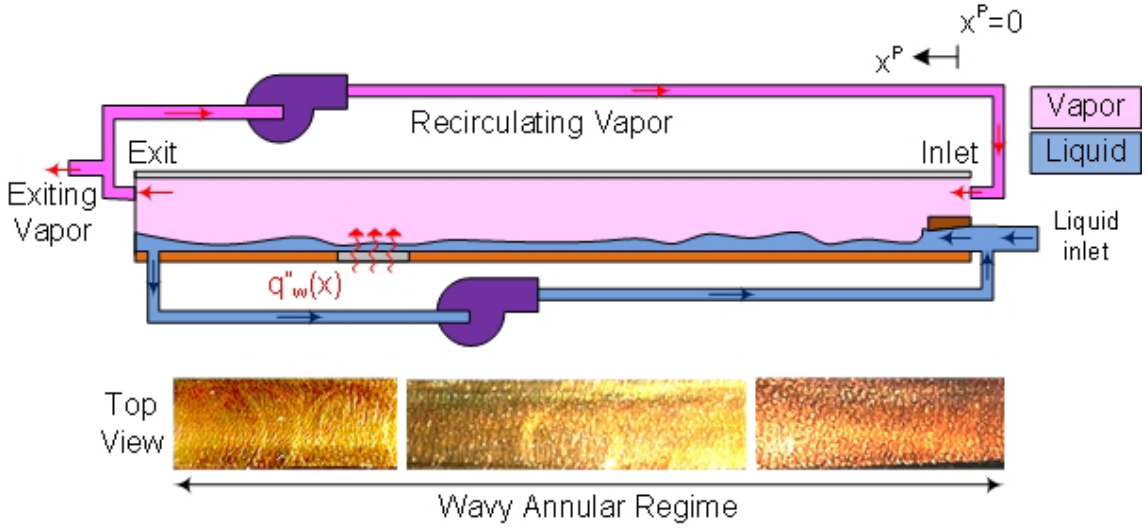

***Fig. 1.1**: Innovative boiler's [1] non-pulsatile operation. Used with permission, see Appendix A3 for copyright license.*

Annular flow boiling regimes (with or without nucleation) also occur in most traditional flow boiling operations (see Fig. 1.2) involving liquid only inlet (at saturation or slightly subcooled temperatures) and vapor only exit.

This thesis directly enables design of innovative flow boiling operations (Fig. 1.1 and [1]) for the non-pulsatile case and indirectly, through forthcoming results, also enables design of very high heat flux gravity-insensitive innovative flow boiling operations for the pulsatile cases as well.

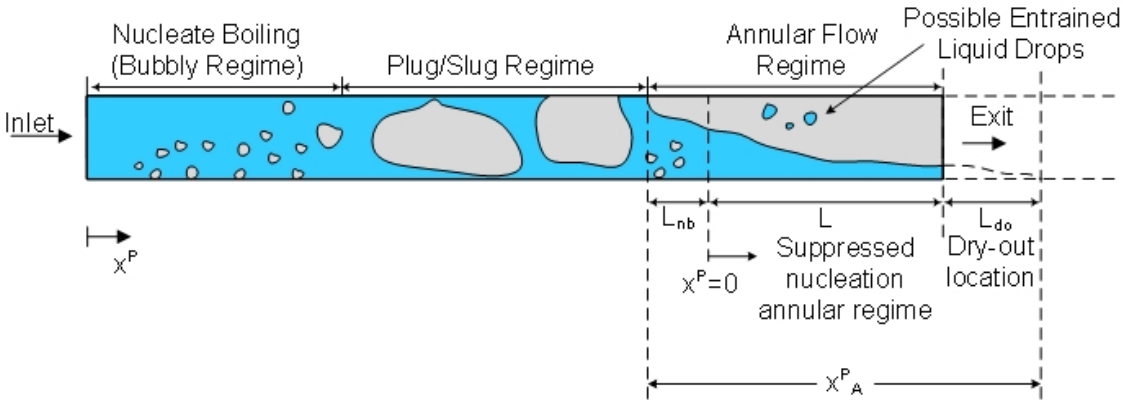

***Fig. 1.2**: A schematic of a traditional flow-boiling operation in a channel with bottom wall heating.*

The broader context [2, 3] of traditional flow-boiling operations in Fig. 1.2 deal with issues such as: different "methods of heating," multiple flow regimes resulting from competing effects of nucleation and convection, effects of gravity, effects of hydraulic diameter of the duct, surface-liquid-vapor interactions (associated with wettability, intermolecular forces, nano- and/or micro-structures present on the surface, etc.), and mechanisms of *critical heat-flux* (CHF). These are typically investigated and explored by a mix of experimental and modeling approaches - with a predominant focus on experiments with uniform heat-flux "method of heating" (see [4-7]) and development of correlations for *heat-transfer-coefficient* (HTC) and pressure drop (see [8-11])

Although direct numerical simulations [12-16] in support of scientific investigation of nucleate pool boiling [2, 3] has been advancing for some time, there are limited literature and analytical techniques on annular flow-boiling (except some that also include other flow regimes, integral methods, and/or correlations based estimates [17-22]). The available results/tools cannot reliably support the design of millimeter-scale innovative boiler operations [1, 23]. Furthermore available numerical or experimental studies [24-27] of external gravity driven falling film evaporation are not applicable to shear-driven evaporative flow-boiling under consideration.

Adapting and utilizing the ability of the reported steady/unsteady simulation techniques for steady internal condensing flows [28-30], this thesis shows that it is now possible to use computational methods to obtain solutions and develop correlations for steady annular flow-boiling situations. Also, the thesis shows that its *direct numerical simulations* (DNS) – a first-principles based subset of *computational fluid dynamics* (CFD) - based correlations (with possible empirical corrections coming from planned synthesis with experiments) can be used to develop simplified predictive tools in support of experiments and design of non-pulsatile annular flow-boiler operations (part of innovative operations [1, 31]).

The nearly exact 2-D steady annular (suppressed nucleation cases) laminar/laminar simulation approach and results, as presented in this paper, enable in addressing some critical issues with regard to flow physics understanding as well as development and usage of *heat transfer coefficient* (HTC) correlations. The thesis enables another thesis [32] which proposes a sample HTC correlation in a well-defined range of non-dimensional numbers

and discusses the validity (while improving the understanding and associated techniques) of popular one-dimensional correlations-based prediction tools. Furthermore, the other forthcoming thesis [32] relying on analogy with stability analyses for annular flow-condensation [29, 30] and additional later discussions in this paper, signatures present in the nearly exact steady annular flow-boiling solutions can be used to estimate the lower threshold of vapor quality $X_{cr|NA-A}$ - below which (i.e. $X < X_{cr|NA-A}$) non-annular (typically plug-slug regime) flow regimes are typically observed in (and modeled through) in experiments [1, 10, 31] involving moderate total mass-flux values ($G \leq 100$ kg/m^{2}s) of refrigerants or water in millimeter-scale horizontal ducts.

Besides enabling design of millimeter-scale innovative flow boilers, the thesis also enables future and forthcoming "experiments-simulations" synthesis for developing models. Such a modeling approach (also see section 5 on forthcoming results) can deal with: (i) development of a criterion for onset of suppressed-nucleation annular flow boiling as the liquid film becomes thinner (also see [10, 33]), (ii) semi-empirical modeling of annular flow boiling in larger diameter ducts in the presence of nucleation, (iii) effects of transverse and axial components of gravity, (iv) the dry-out related CHF mechanism (out of at least three-to-four different mechanisms of CHF discussed in the literature [2, 33]) that is typically relevant to the innovative annular flow-boiling ([1] and Fig. 2.1) approach, (v) experimental and computational support for non-annular to annular flow-regime transition criteria based on recently reported instability analyses tools [29, 30] capable of estimating/identifying such conditions, (vi) development of pressure-drop correlations, etc.

Additional "experiments-simulations" synthesis approach will enable development of empirical models that can be superposed on HTC correlations of the type proposed here – and this will yield HTC correlations for the technologically important very high heat-flux pulsatile operations [1]. These operations involve superposition of large-amplitude standing waves on thin film boiling (over hydrophilic or super-hydrophilic surfaces) associated with steady non-pulsatile realizations (for which modeling approach is described in this thesis).

2. Problem Statement and Governing Equations

The computational algorithm and solutions presented here are for steady annular/stratified channel flow boiling (under suppressed nucleation conditions) inside channel as shown in Fig. 2.1. These boiling flows are achieved by heating the bottom wall and keeping the top wall at close to, or slightly above, local vapor saturation temperatures. In Fig. 2.1, gravity driven cases correspond to $\alpha > 0$ and shear driven cases correspond to zero-gravity ($\vec{g} = 0$) or horizontal ($\alpha = 0$) cases. The length L (the distance between inlet and outlet) in Fig. 2.1 typically corresponds to $L \leq x_A^p$, the length of annular regime (which can be defined, as in Fig. 1.2, to be the distance between the modeled "point of transition" between non-annular and annular regimes and either the device's exit or the hypothetical "point of dry-out" - if it lies downstream of the exit).

The two-dimensional computational approach employed to investigate annular flow boiling inside channels and tubes is based on the full governing equations described here. Analogous flow condensation approaches are given in [29, 30].

The liquid and vapor phases in the flow are denoted with subscripts I = 1 and I = 2 (alternatively, as I = 'L' and 'V') respectively. Both phases are modeled as incompressible (i.e. vapor Mach numbers are low). The fluid properties (density ρ, viscosity μ, specific heat C_p, and thermal conductivity k) are denoted with subscript I. The properties are to take their representative constant values for each phase (I = 1 or 2).

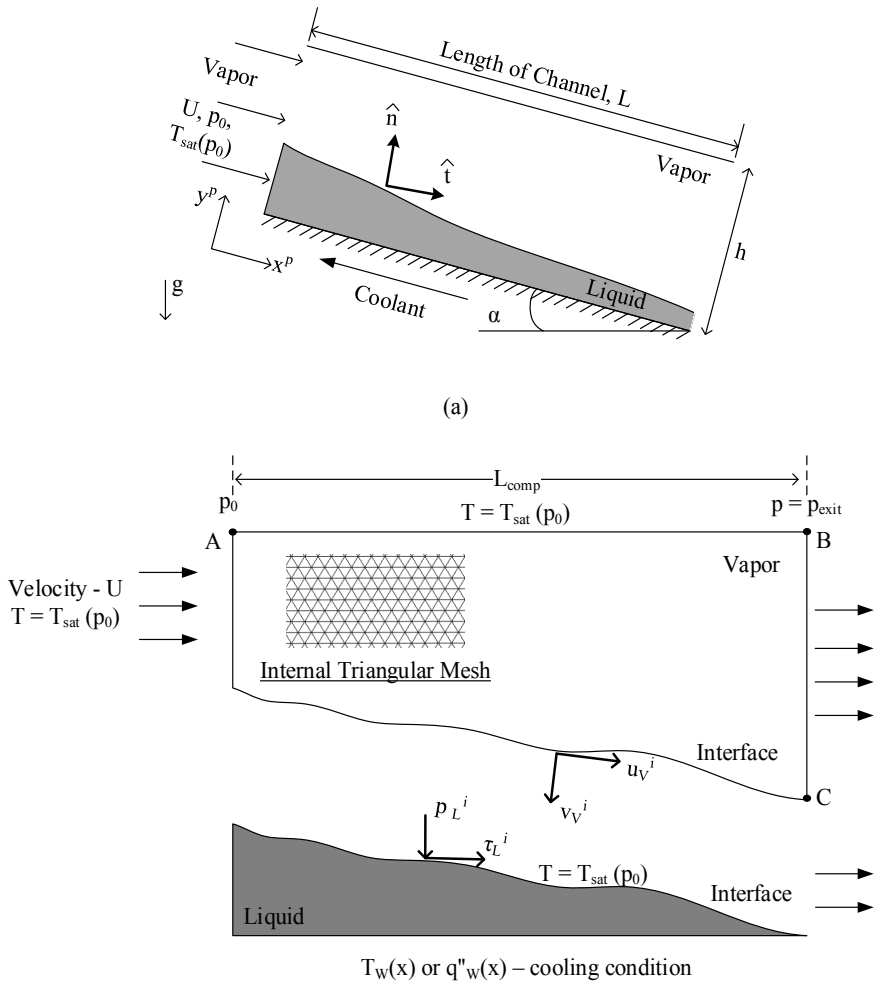

Fig 2.1: (a) *Schematic of a representative suppressed nucleation case of annular flow boiling in a channel.* ***(b)*** *Schematic of a representative instantaneous interface location showing the interfacial variables used as boundary conditions for the liquid and the vapor domains. The computational domain's exit at x = L_{comp} in (b) is often slightly larger than the exit at x = L in (a)*

Let the temperature, pressure, and velocity fields over the two phases be respectively denoted as T_I, p_I, and $\vec{\mathbf{v}}_I = u_I\hat{\mathbf{i}} + v_I\hat{\mathbf{j}}$. Also, let $T_{sat}(p)$ be the saturation temperature of the vapor as a function of local pressure p at the interface, Δ be the film thickness, $\dot{m}^p$ be the local interfacial phase- change mass flux (kg/m^2-s), and $T_w(x)$ (> $T_{sat}(p)$) be a known

temperature variation of the heated bottom surface (with its length-averaged mean value being $\overline{T}_W$, where $\overline{T}_w \equiv {}^{1}\!/_{L} * \int_0^L T_w(x)dx$). Let g_x and g_y be the components of gravity along the x and y axes, p_0 be the steady inlet pressure, ΔT ($\equiv \overline{T}_W - T_{sat}(p_0)$) be a representative controlling temperature difference between the liquid and the bottom plate, h_{fg} be the heat of vaporization at temperature $T_{sat}(p)$, and U be the average inlet vapor speed determined by the inlet mass flow rate per unit width $\dot{M}_{in}$ ($\equiv \rho_2 \bullet U \bullet h$, where $\dot{M}_{in} = \dot{M}_{in}.w$ is the inlet mass flow rate for rectangular cross-section channel of height h and width w, provided h/w << 1). Let (x^p, y^p) represent physical distances of a point with respect to the axes in Fig. 2.1 (for which $x^p = 0$ is at the inlet and $y^p = 0$ is at the heated bottom wall surface). Next a new list of fundamental non-dimensional variables, ($x, y, t, \delta, u_I, v_I, \pi_I, \theta_I, \dot{m}$) are introduced through the following definitions:

$$[\, x^p, y^p, \Delta, u_I^p, v_I^p \,] \equiv [\, h.x, h.y, h.\delta, U.u_I, U.v_I] \qquad (2.1)$$

$$[\, \dot{m}^p, T_I, p_I] \equiv [\rho_1.U.\dot{m}, T_{sat}(p_0)+\Delta T.\theta_I, p_0 + \rho_I.U^2.\pi_I]$$

The above annular flow-boiling specification is appropriate for prescribed or known wall temperatures $T_w(x)$ for a given "method of heating." In this case, boiling surface heat-flux $q''_w(x)$ and local heat transfer coefficient $h_x (\equiv q''_w(x)/\Delta T)$ are values to be found as part of the CFD solution. For prescribed heat flux method of heating $q''_w(x)(\equiv \overline{q''_w}.\Psi_q(x))$ values are known. This is equivalent to knowing the mean-heat flux $\overline{q''_w} \equiv {}^{1}\!/_{L} * \int_0^L q''_w(x)dx$ value

and associated "method of heating" characterization function $\Psi_q(x)$. In this case, $T_w(x)$, $\overline{T}_w$ and ΔT are the quantities that are obtained as part of the CFD solution.

The representative constant values of the fluid properties are obtained from Engineering Equation Solver (EES) software [34] and other data handbooks. However, there are some inherent uncertainties associated with experimental data reported in the handbook values. Therefore, key results presented in non-dimensional terms should be assumed to have some additional uncertainties associated with fluid properties (appearing in non-dimensional parameters) over and above computational error uncertainties (associated with level of convergence, discretization/truncation errors, etc.).

2.1. Interior Equations

The differential forms of mass, momentum (x^p and y^p components), and energy equations for 2-D flow in the interior of both the incompressible phases are the well-known equations (see [30]) presented in Eq. 2.2 below.

The simulations emphasized here assume laminar vapor and laminar liquid flows. For most shear driven flows of interest to mm-scale boilers, the laminar liquid flow assumption holds up to the end of the computational domain (i.e. the distance in Fig. 1.1 between the inlet, $x^p = 0$, and the exit, $x^p = L$ – where L is typically less than the length x_A^p of the annular regime, also see corresponding locations in Fig. 1.2). It is expected that the comparisons of results obtained from these simulations with corresponding experimental results for suppressed nucleation cases will be quite good even if the vapor flow *far* from the near interface zone (connected with the laminar liquid flow) is turbulent (as indicated by local

values of vapor-phase Reynolds number). This agreement is expected because dominant values of near-interface vapor flow variables, e.g., x and y components of the interfacial vapor velocity, will remain very small and locally laminar as the liquid flow remains thin and dominated by viscous forces. Any additional randomness introduced through interfacial waviness arising from far field vapor core turbulence may, at most, contribute to "laminar interfacial turbulence" but this will not have sufficient impact on the significantly stronger instability mechanisms (see analogous discussion in [29, 30] for condensing flows) that yield an estimate for the length $x_A \equiv x_A^P/h$ of the annular regime.

Under laminar/laminar assumption, the non-dimensional differential forms of mass, momentum (x and y components), and energy equations for the two-dimensional flow in the interior of either of the incompressible phases (I = 1 or 2) are the well-known equations:

$$\frac{\partial u_I}{\partial x}+\frac{\partial v_I}{\partial y}=0$$

$$\frac{\partial u_I}{\partial t}+ u_I\frac{\partial u_I}{\partial x}+ v_I\frac{\partial u_I}{\partial y}=-\left(\frac{\partial \pi_I}{\partial x}\right)+ Fr_x^{-2}+\frac{1}{Re_I}\left(\frac{\partial^2 u_I}{\partial x^2}+\frac{\partial^2 u_I}{\partial y^2}\right)$$

$$\frac{\partial v_I}{\partial t}+ u_I\frac{\partial v_I}{\partial x}+ v_I\frac{\partial v_I}{\partial y}=-\left(\frac{\partial \pi_I}{\partial y}\right)+ Fr_y^{-2}+\frac{1}{Re_I}\left(\frac{\partial^2 v_I}{\partial x^2}+\frac{\partial^2 v_I}{\partial y^2}\right) \qquad (2.2)$$

$$\frac{\partial \theta_I}{\partial t}+ u_I\frac{\partial \theta_I}{\partial x}+ v_I\frac{\partial \theta_I}{\partial y}\approx\frac{1}{Re_I.Pr_I}\left(\frac{\partial^2 \theta_I}{\partial x^2}+\frac{\partial^2 \theta_I}{\partial y^2}\right)$$

where $Re_I \equiv \rho_I U h/\mu_I$, $Pr_I \equiv \mu_I C_{pI}/k_I$, $Fr_x^{-2} \equiv g_x h/U^2$ and $Fr_y^{-2} \equiv g_y h/U^2$.

2.2. Interface Conditions

Superscript "i" is used for the values of flow variables at the interface. The interface, is explicitly located by the expression $\Phi \equiv y^p - \Delta(x^p) = 0$. The nearly exact interface conditions (see [30, 35, 36] etc.) are better qualified, extended (to cover sub-micron condensate thickness values of current interest as well as for planned future investigations), and re-stated here in Appendix A1. The "Newtonian" fluid models for stresses $\mathbf{T}_1$ and $\mathbf{T}_2$ defined in Appendix A1 also define the values of the vapor and liquid phases' traction vectors $\vec{\tau}_2^{pi}$ and $\vec{\tau}_1^{pi}$ at any point on the interface ($\Phi = 0$). At any point on the interface, the unit normal (directed from the liquid to the vapor phase) is denoted by $\hat{\mathbf{n}}$ and unit tangent vector by $\hat{\mathbf{t}}$. Note that traction vectors (see Appendix A1 or [36]) $\vec{\tau}_2^{pi} \equiv \mathbf{T}_2^i\hat{\mathbf{n}} \equiv \tau_{2x}^{pi}\hat{\mathbf{i}} + \tau_{2y}^{pi}\hat{\mathbf{j}} \equiv -p_2^i\hat{\mathbf{n}} + \tau_2^{pi}\hat{\mathbf{t}}$ and $\vec{\tau}_1^{pi} \equiv \mathbf{T}_1^i\hat{\mathbf{n}} \equiv \tau_{1x}^{pi}\hat{\mathbf{i}} + \tau_{1y}^{pi}\hat{\mathbf{j}} \equiv -p_1^i\hat{\mathbf{n}} + \tau_1^{pi}\hat{\mathbf{t}}$. The non-dimensional values of the stress vector components are, respectively, defined as $\vec{\tau}_2^{\,i} \equiv (h/\mu_2 U).\vec{\tau}_2^{pi} \equiv \tau_{2x}^i\hat{\mathbf{i}} + \tau_{2y}^i\hat{\mathbf{j}}$ and $\vec{\tau}_1^{\,i} \equiv (h/\mu_1 U).\vec{\tau}_1^{pi} \equiv \tau_{1x}^i\hat{\mathbf{i}} + \tau_{1y}^i\hat{\mathbf{j}}$. *Non-dimensional* Cartesian co-ordinate forms of the interface conditions, for the flow in Fig. 2.1, are given below:

- The continuity of tangential component of velocities is a requirement (see Eq. (A1.2)). This requirement non-dimensionalizes, under Eq. (3.1), to:

$$u_2^i = u_1^i - \delta_x\left(v_2^i - v_1^i\right) \tag{2.3}$$

where $\delta_x \equiv \partial\delta/\partial x$.

- The normal component of momentum balance at the interface, after ignoring the normal component of viscous stresses in comparison to interfacial pressures, is modeled by Eq. (A1.3) in Appendix A1. This relationship non-dimensionalizes to:

$$\pi_1^i = \frac{\rho_2}{\rho_1}\pi_2^i - \frac{1}{We}\left(\frac{\delta_{xx}}{\left[1+\delta_x^2\right]^{3/2}}\right) + \dot{m}^2\left(\frac{\rho_1}{\rho_2}-1\right), \tag{2.4}$$

where $We \equiv \rho_1 U^2 h/\sigma$ and surface tension σ for the pure vapor depends on local interfacial temperature T^i (i.e. $\sigma = \sigma(T^i)$).

- The tangential component of momentum balance at the interface (see Eq. (A1.4)) non-dimensionalizes to:

$$\left.\frac{\partial u_1}{\partial y}\right|^i = \frac{\mu_2}{\mu_1}\left.\frac{\partial u_2}{\partial y}\right|^i + [t], \tag{2.5}$$

where the term [t] in Eq. (2.5) is defined as:

$$[t] = \left\{\frac{\mu_2}{\mu_1}\left.\frac{\partial v_2}{\partial x}\right|^i - \left.\frac{\partial v_1}{\partial x}\right|^i\right\} + \frac{2\delta_x}{\left[1+\delta_x^2\right]}\left\{\left.\frac{\partial u_1}{\partial x}\right|^i - \left.\frac{\partial v_1}{\partial y}\right|^i\right\} - \frac{2\delta_x}{\left[1+\delta_x^2\right]}\frac{\mu_2}{\mu_1}\left\{\left.\frac{\partial u_2}{\partial x}\right|^i - \left.\frac{\partial v_2}{\partial y}\right|^i\right\} \tag{2.6}$$

Following discussions given for Eq. (A1.4), the right side of Eq. (2.6) has ignored the Marangoni term (whose effects, for the class of problems studied here, are known to be negligible).

- The non-dimensional form of non-zero physical values of interfacial mass fluxes $\dot{m}_{LK}^p$ and $\dot{m}_{VK}^p$ (defined in Eq. (A1.5)) arise from kinematic constraints associated with the liquid and vapor velocity values at the interface. In the non-dimensional form these are given by:

$$\dot{m}_{LK} \equiv \left[-u_1^i \left(\frac{\partial \delta}{\partial x} \right) + \left(v_1^i - \frac{\partial \delta}{\partial t} \right) \right] / \sqrt{1 + \left(\frac{\partial \delta}{\partial x} \right)^2} \quad \text{and}$$

$$\dot{m}_{VK} \equiv \frac{\rho_2}{\rho_1} \left[-u_2^i \left(\frac{\partial \delta}{\partial x} \right) + \left(v_2^i - \frac{\partial \delta}{\partial t} \right) \right] / \sqrt{1 + \left(\frac{\partial \delta}{\partial x} \right)^2} \, . \tag{2.7}$$

- The non-dimensional form of non-zero physical values of interfacial mass flux $\dot{m}^p_{Energy}$ (as given by Eq. (A1.6)) represents the constraint imposed by the dominant net thermal energy transfer rates across the interface and is given by:

$$\dot{m}_{Energy} \cong \frac{Ja}{Re_l Pr_l} \left\{ -\frac{\partial \theta_1}{\partial n}\bigg|^i + \frac{k_2}{k_1} \frac{\partial \theta_2}{\partial n}\bigg|^i \right\}, \tag{2.8}$$

where $Ja \equiv C_{p1} \cdot \Delta T / h_{fg}$ and $h_{fg} \equiv h_{fg}(T_{sat}(p_2^i))$. Recall that liquid Reynolds number Re_l and Prandtl number Pr_l are given by their definitions that immediately follow Eq. (2.2).

For the case of prescribed heat flux ($q''_w(x) = \overline{q''_w} . \Psi_q(x)$) – with average value heat flux of $\overline{q''_w}$ over $0 \le x \le L$ - Eq. (A1.6) in Appendix A1 can be used to rewrite Eq. (2.8) in its alternative non-dimensional form:

$$\dot{m}_{Energy} = \frac{\overline{q''_w}}{\rho_2 U h_{fg}} . \frac{\rho_2}{\rho_1} . \Psi_q(x) \equiv Bl . \frac{\rho_2}{\rho_1} . \Psi_q(x) \tag{2.9}$$

where $Bl \equiv \overline{q''_w} / (\rho_2 U h_{fg})$ & $\Psi_q(x) \equiv q''_{int}(x) / \overline{q''_w}$. Here interfacial heat-flux $q''_{int}(x)$ is in the normal $\hat{\mathbf{n}}$ direction at any point (associated with distance x and associated position vector **x** on the interface) and equals $\dot{m}^p_{Energy} . h_{fg}$ where $\dot{m}^p_{Energy}$ is given by Eq. (A1.6). However for thin film flows of interest to this paper, the relationship $q''_{int}(x) = q''_w(x)$ holds.

- The interfacial mass balance (in Eq. (A1.9) or, when necessary, by Eq. (A1.10)) requires that the net mass flux (in kg/m^2-s) at a point on the interface, must be the same for all the different physical processes that impose a constraint on its local value. The non-dimensional form of this requirement becomes:

$$\dot{m}_{LK} = \dot{m}_{VK} = \dot{m}_{Energy} \equiv \dot{m} \tag{2.10}$$

It should be noted that negligible interfacial thermal resistance and equilibrium thermodynamics is assumed to hold on either side of the interface. This is reasonable, except for some situations discussed in Appendix A1. This is because the liquid film thickness values considered here are typically greater than a few micrometers and less than, or at most, same order as the millimeter scale channel height h. This modeling assumption typically holds for almost all "x" values of interest ($0 \le x \le L$) over which the CFD solution is sought.

- The non-dimensional thermodynamic restriction on interfacial temperatures (as given by the approximation in Eq. (A1.7), becomes:

$$\theta_1^i \cong \theta_2^i \equiv \theta_s\left(\pi_2^i\right). \tag{2.11}$$

Within the vapor phase, for the refrigerants and millimeter scale ducts considered here, the inlet pressure $p_0 << p_{cr}$, where p_{cr} is the critical pressure [3] of the vapor. As a result, the changes in absolute pressure relative to the inlet pressure are big enough to affect vapor motion but, at the same time, they are usually too small to significantly affect saturation temperatures (except in micro-scale ducts and at high mass flux G). Therefore, computations also show that, we have $\theta_s\left(\pi_2^i\right) \cong \theta_s\left(0\right)$.

2.3. Boundary Conditions for Combined Consideration of the Vapor and Liquid Domains

The problem is computationally solved subject to the boundary conditions shown on a representative and not-to-scale, film profile in the vapor-liquid domain of Fig. 2.1b.

Top wall: The upper wall physical temperature $T_2(x^p,h) > T_{sat}(p_o)$ is at a superheated value (typically 5-10°C above saturation temperature) and this, along with $p_0 << p_{cr}$ assumption, makes the vapor solutions almost indistinguishable from those that assume vapor phase temperature to be a uniform $T_{sat}(p_0)$.

Bottom wall: Besides the no-slip condition at the boiling surface, a steady boiling surface temperature $T_1(x^p,0) = T_w(x^p)$ ($> T_{sat}(p_0)$) - or a steady wall heat flux $q''_w(x)$ - define its *thermal* boundary condition. Also, as experimentally established ([23]), a *specific* non-dimensional temperature function:

$$\theta_w(x) \equiv \theta_1(x,0) = \frac{T_1(x,0) - T_{sat}(p_0)}{\overline{T}_w - T_{sat}(p_0)} \tag{2.12}$$

for wall temperature $T_w(x^p)$ - or a *specific* $\Psi_q(x)$ in the wall heat flux prescription $q''_w(x) \equiv \overline{q''_w}.\Psi_q(x)$ - define a *specific* "method of heating."

Inlet conditions and significance of its resolution: At the inlet ($x^p = 0$), presence of evaporative annular flow boiling (Fig.2.1a) is assumed, and one requires among other

variables, a prescription of a finite non-zero film thickness, $\Delta(0) = \Delta_{in}$. Because of the finiteness of Δ_{in} (unlike $\Delta_{in} \cong 0$ in the onset of condensation condition discussed in [30, 36]), this value has to be "special" as all inlet variable profiles – such as inlet liquid velocity, pressure and temperature profiles ($u_1(0,y)$, $v_1(0,y)$, $p_1(0,y)$, $T_1(0,y)$ over $0 \le y \le \Delta_0$), inlet vapor velocity, pressure and temperature profiles ($u_2(0,y)$, $v_2(0,y)$, $p_2(0,y)$, $T_2(0,y)$ over $\Delta_0 \le y \le h$), inlet values of interfacial stress vectors ($\vec{\tau}_1^{pi}(x^p = 0, y^p = \Delta_0)$, $\vec{\tau}_2^{pi}(x^p = 0, y^p = \Delta_0)$), and interfacial mass flux ($\dot{m}^p(x^p = 0, y^p = \Delta_0)$) – have to be "mutually consistent" (satisfy all the interfacial conditions) for the proposed laminar/laminar simulations. Such restrictive compatibility requirements among so many variables make full 2-D annular flow boiling simulations a challenge – particularly when one compares it with simpler correlations-based one-dimensional (1-D) simulations/models for annular boiling (to be described in Section 3.3) which only requires prescriptions of total mass flow rate per unit width and inlet thermodynamic quality at $x^p = 0$. That is, for correlations-based simpler calculations, only total mass flow rate per unit width $\dot{M}_{in} \equiv \dot{M}_L(0) + \dot{M}_V(0) \equiv \int_0^{\Delta_0} \rho_1 \cdot u_1^p(0, y^p) \cdot dy^p + \int_{\Delta_0}^{h} \rho_2 \cdot u_2^p(0, y^p) \cdot dy^p$) and inlet quality is $X_{in} \equiv X(0) = \dot{M}_V(0) / \dot{M}_{in}$ are needed at $x^p = 0$. Therefore it is expected that, perhaps, detailed inlet conditions information for the two-dimensional (2-D) steady simulation are only very important to implement DNS. The usefulness of DNS also lies in the processed one-dimensional values (and their correlations) that it yields for the local HTC h_x. The paper shows that the 1-D calculations based on CFD-enabled HTC correlations are indeed relatively insensitive to such details with regard to inlet condition.

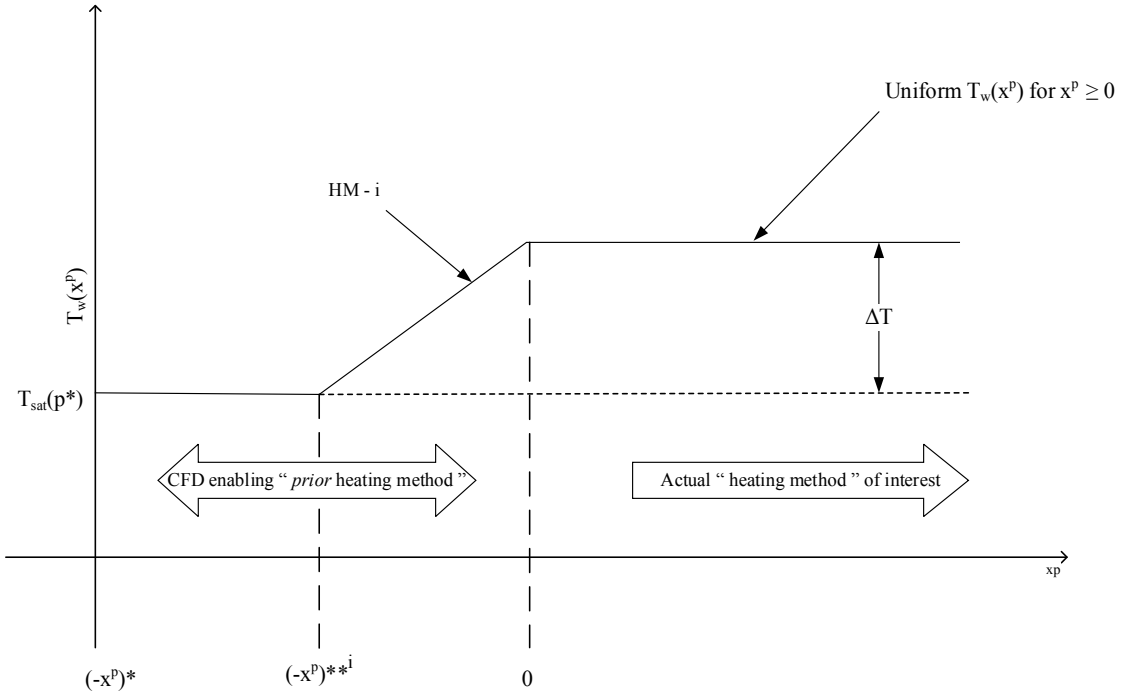

(a)

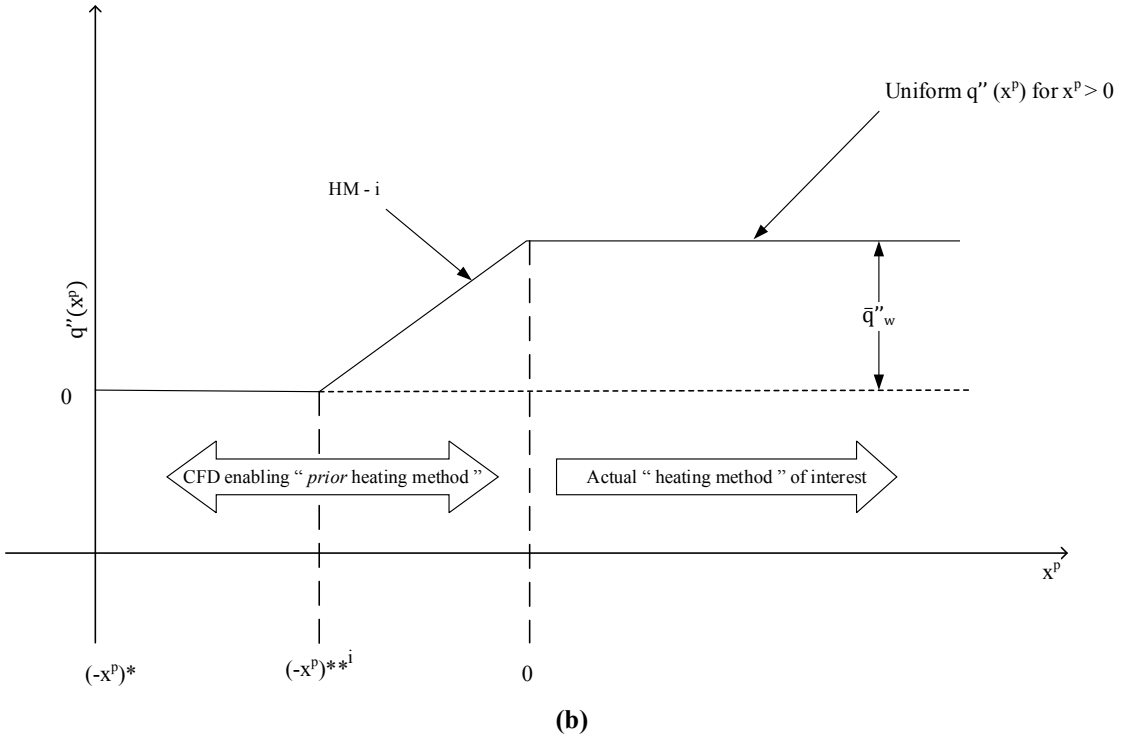

(b)

Fig. 2.2 (a) *Representative Wall temperature ($T_w(x)$) prescribed "methods of heating" over $x^p \geq 0$ & $-x^{p^*} < x^p < 0$.* ***(b)*** *Representative wall heat flux ($q''_w(x)$) prescribed "methods of heating" over $x^p \geq 0$ & $-x^{p^*} < x^p < 0$*

To benefit from detailed CFD solution and to address the needs of this rather restrictive specification of inlet conditions, the following *enabling* approach is recommended. The proposed *enabling* approach to deal with this situation is that a "prior method of heating" be prescribed (see Figs. 2.2a-b) for $x^p < 0$. Whether it is wall temperature $T_w(x)$ (Fig 2.2a) or wall heat flux $q''_w(x)$ (Fig 2.2b) prescription, at a certain $x^p = -x^{p*}$, it is assumed that liquid and vapor enter the channel as adiabatic isothermal laminar/laminar flows (i.e., both phases are at same uniform temperature and experience no active heating over a certain adiabatic zone, viz. $-x^{p*} < x^p < -x^{p**}$). For this adiabatic zone, "mutually consistent" analytical prescriptions for all required inlet-conditions are available at $x^p = -x^{p*}$ (see Appendix A2).

At the location $x^p = -x^{p*}$ in Figs. 2.2a-b, the fluid temperatures and wall temperatures all equal $T_{sat}(p^*)$, where p* is the absolute pressure assumed for the top wall location at $x^p = -x^{p*}$. At $x^p = -x^{p*}$, the consistent values of liquid and vapor phases' velocity, pressure and temperature profiles; interfacial stress vectors; and interfacial mass flux are as given in Appendix A2. For any assumed "heating method" (denoted as "HM-i", i = 1, 2 & 3 in the caption of Figs. 2.2a-b), mass flow rate $\dot{M}_{in}$, and suitably assigned inlet conditions such as quality values at $x^p = -x^{p*}$ associated with liquid and vapor flow rates - $\dot{M}_L(x^p = -x^{p*})$ and $\dot{M}_V(x^p = -x^{p*})$ respectively, the CFD solution over $x^p > -x^{p*}$ automatically yields correct and consistent inlet conditions for the heated location of interest which begins at $x^p = 0$. The actual physical value of the steady pressure p_{in} (= p_0)

at $x^p = 0$ is not directly used in CFD but it indirectly appears through fluid properties and important thermodynamic properties such as $h_{fg}(p_2^i) \approx h_{fg}(p_0)$ and $T_{sat}(p_2^i) \approx T_{sat}(p_0)$.

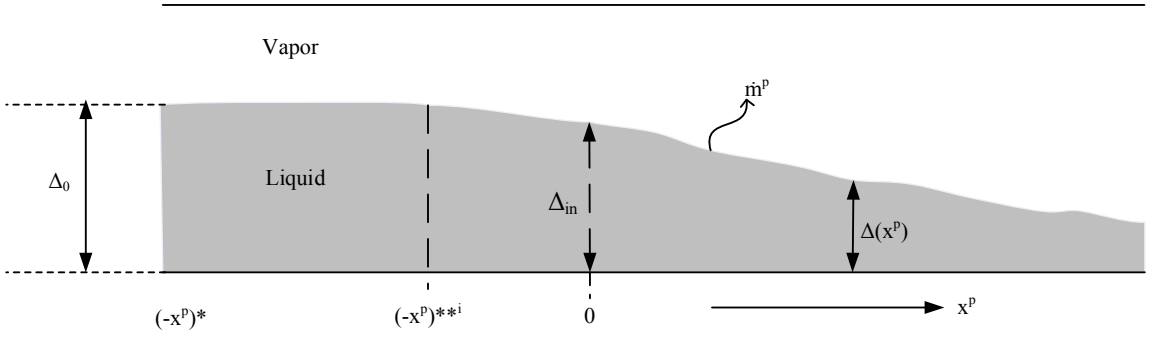

Fig. 2.3 *Representative film thickness profile for "method of heating" in Fig 2.2*

Steady Exit conditions: For the steady problem, the flow is parabolic and no exit condition is needed. Pressure is not directly prescribed across the exit boundary for the computational simulations. Its arbitrary "reference" value p_{exit} is specified, to begin with, in the vapor domain – at the corner point of the intersection of the exit and the top wall (point B in Fig 2.1b). This value is then re-adjusted to ensure a reference pressure value of $p_{ref}|_A = 0$ for the reference location point A (at x = 0 in Fig. 2.1b).

Initial Conditions: The steady problem considered here needs no initial condition prescription associated with time t = 0. It does, however, require some reasonable but arbitrary initial values for the first iteration, as described in step (i) of the algorithm in section 3 below.

3. Computational Approach and Algorithm

The 2-D steady computational algorithm will be described for obtaining steady solutions of the steady boundary value problem shown in Fig. 2.1b. The solution can be obtained by the steady approach described below.

The simulation uses an approach of separately solving, on COMSOL, the (steady) liquid and vapor domain governing equations over their respective domains – domains that result from the assumed "sharp" interface model in Fig. 2.1b. The steady algorithm - after making choices for the gap height h, the pure fluid, inlet pressure p_0, and cooling conditions – obtains fluid properties, sets $\theta_l^i \cong \theta_s(0)$, and begins with assuming reasonable first-guess values of interface location function $\Delta(x)$ (or non-dimensional $\delta(x)$) along with key interfacial flow variable functions $u_l^i(x)$ and $\dot{m}(x)$ (where $\dot{m}$ is for obtaining $v_l^i(x)$ values). The steady single domain *direct numerical solution* (DNS) approach for each of the two phases retains all the steady terms in the governing equations (including interface conditions) of section 2 - except that, to model steady flows, all partial time derivatives are set to zero.

The approach used here for annular suppressed nucleation steady flow boiling is essentially the same as the steady algorithm for annular flow condensation described in [29, 30]. With respect to Fig. 2.1, the algorithm consists of the following steps:

(i) Utilizing the liquid side interfacial flow variables first guesses of u_l^i, v_l^i, θ_l^i and the first guess of steady film thickness $\delta(x)$, the liquid domain in Fig. 2.1b is treated as a separate "fixed" domain and the governing interior equations of mass, momentum

and energy are solved on COMSOL. The exit boundary at x = L_{comp} is treated as one of known arbitrary first guess uniform pressure which equals the corner pressure (i.e., $p_1\left(L_{comp},\ y\right) \cong p_1^i(L_{comp}, y) \equiv p_{ref}$). The boundary conditions for the interface is one which has the prescribed aforementioned first guess values of velocity (u_1^i, v_1^i) and temperature (θ_1^i). The two-phase flow simulations' inlet of interest at x = 0 is extended upstream to a *de facto* inlet at $x^p = -x^{p^*}$, which is associated with known adiabatic flow conditions. The bottom wall thermal boundary conditions for the x < 0 zone are as prescribed in Fig. 2.2a or 2.2b. The uniform temperature and velocity profiles $u_1(x^p = -x^{p^*}, y)$ and $v_1(x^p = -x^{p^*}, y)$ - all are available from analytically known adiabatic flow results (for any appropriate liquid mass flow rate $\dot{M}_L$ and associated film thickness $\Delta_0 = \Delta(x^p = -x^{p^*})$, these are obtained as per procedures given in Appendix A2). The COMSOL solution at this step is used to yield reasonable first guess values of interior liquid domain flow variables, viz. $u_1(x,y)$, $v_1(x,y)$, $\pi_1(x,y)$, and $\theta_1(x,y)$.

(ii) Next, continuity of tangential velocity (Eq. 2.3) and $\dot{m}_{LK} = \dot{m}_{VK}$ (part of Eq. 2.10) with terms as in Eq. 2.7 are used to obtain $u_2^i(x)$ and $v_2^i(x)$ values. The non-dimensional temperature, $\theta_2^i(x)$ is obtained from Eq. 2.11. The mathematical operations for obtaining these functions are performed within a MATLAB program and results are transferred to COMSOL.

(iii) Utilizing the currently available location δ(x) and vapor side interfacial flow variables u_2^i, v_2^i, and θ_2^i obtained through the previous step; the temporarily (for

this iteration) "fixed" vapor domain in Fig 2.1b is used to solve the interior governing equations of mass, momentum and energy on COMSOL. Here, the interface is one of the boundaries which has prescribed velocity components and temperature conditions. The exit at x = L_{comp} is treated as prescribed outflow boundary condition with zero reference pressure at point B of Fig 2.1b. The upstream extended inlet at $x^p = -x^{p*}$ (with bottom wall thermal boundary conditions for the liquid as in Fig. 2.2a and 2.2b) – also has known velocity profiles for u_2 or v_2 at $x^p = -x^{p*}$. These are associated with the adiabatic flow results for vapor mass flow rate of $\dot{M}_V = \dot{M}_{in} - \dot{M}_L$, and film thickness $\Delta_0 = \Delta(x^p = -x^{p*})$ - and all these results are given in Appendix A2. The computationally predicted velocity profiles of $u_2(x,y)$, $v_2(x,y)$ are retained and pressure profile $\pi_2(x,y)$ is re-adjusted so as to make the reference pressure zero at point A ($x^p = -x^{p*}$) instead of at point B in Fig. 2.1b. Next, COMSOL is used to obtain the x and y components of stress vector $\vec{\tau}_2^{pi}$ or its non-dimensional value $\vec{\tau}_2^{i}$.

(iv) Using the normal and tangential components of interfacial momentum balance conditions (Eqs. 2.4 and 2.5) along with the x and y components of the computed values of $\vec{\tau}_2^{i}$ in step (iii) above, MATLAB is used to obtain the x and y components of the liquid side's interfacial stress vector $\vec{\tau}_1^{pi}$ and its non-dimensional value $\vec{\tau}_1^{i}$.

(v) Using the stress components of $\vec{\tau}_1^{i}$ at the interface of the liquid domain as boundary condition to replace the velocity components (u_1^i, v_1^i), while retaining the remaining prescriptions associated with step (i); the liquid domain problem is re-solved on COMSOL for $-x^{p*} < x^p < L_{comp}$ -with bottom wall thermal boundary condition as in

Fig. 2.2a or 2.2b. Key variables from the resulting solution are saved. These are interior liquid domain values of the variables u_1, v_1, π_1 and θ_1, - as well as their interfacial values associated with the one-dimensional interfacial functions u_1^i and v_1^i.

(vi) At this point all the interfacial conditions in section 2.2, except the remaining equality of Eq. 2.10, viz.: $\dot{m}_{LK} = \dot{m}_{Energy}$, has been satisfied. As discussed in Ranjeeth et al. ([29, 30]), this equality leads to an interface tracking equation whose steady form is:

$$\frac{d\delta(x)}{dx} = \frac{\overline{v}}{\overline{u}}, \; x^p \geq -x^{p^*} \tag{3.1}$$

Where, $\delta(-x^{p^*}) = \delta_0 \equiv \Delta_0/h$ is known from Appendix A2's Eqs. (A2.10) - (A2.11). For prescribed temperature boundary conditions, the definitions of $\overline{u}(x)$ and $\overline{v}(x)$ in Eq (3.1) arise from use of Eq. (2.8) for $\dot{m}_{Energy}$. This yields:

$$\begin{aligned} \overline{u} &\equiv u_1^i + \left[Ja/(Re_1.Pr_1)\right]\partial\theta/\partial x\Big|^i \\ \text{and, } \overline{v} &\equiv v_1^i + \left[Ja/(Re_1.Pr_1)\right]\partial\theta/\partial x\Big|^i \end{aligned} \tag{3.2}$$

For prescribed heat-flux boundary-conditions, the definitions of $\overline{u}(x)$ and $\overline{v}(x)$ in Eq. (3.1) arise from use of Eq. 2.9 for $\dot{m}_{Energy}$. This leads to:

$$\begin{aligned} \overline{u} &\equiv u_1^i \\ \text{and, } \overline{v} &\equiv v_1^i + Bl.\frac{\rho_2}{\rho_1}.\Psi_q(x) \end{aligned} \tag{3.3}$$

Next, on MATLAB, Eq. 3.1 is solved by a simple numerical integration scheme (trapezoidal Simpson rule or higher order, as needed) to yield a new estimate of the interface location $\delta(x)$ for a certain discretization of the x-axis, where $x = x_i = i.(\Delta x_{f\text{-}g})$ (with integer i = 0, 1, 2…). At this point in the algorithm, the location of $\delta(x)$ is updated after Eq. 3.1 is solved, and the changed location is used to change the domain (by a simple mapping technique) of all the previously computed interior liquid domain variables u_1, v_1, π_1, etc. available over $-x^{p^*} < x^p < L_{comp}$ from their earlier y-domain to this step's new y-domain of $0 \le y \le \delta(x)$.

(vii) With the updated liquid domain solution and interface location from step (vi) above, steps (ii) through (vi) are repeated until converged solutions are obtained. Besides COMSOL's convergence tests for numerical solutions of interior equations for each of the two-phases, it is checked that all interior, interface, and boundary conditions are satisfied.

In the implementation of the above algorithm, a COMSOL-specific point with regard to post solution evaluation of interfacial stress vector $\vec{\tau}_2^{pi}$ in step (iii) above should be noted. The x and y components, τ_{2x}^p and τ_{2y}^p are directly and concurrently evaluated in COMSOL at any interior "$x = x_i$" where $-x^{p^*} < x_i < L_{comp}$. It appears that COMSOL's default procedure is to obtain these values by a higher order central differencing type approach (i.e. utilizes values at x_{i-1}, x_{i+1}, etc.) at an interior x-location. However, at the left and right boundary points of $x^p = -x^{p^*}$ and $x^p = L_{comp}$, it should be obtained by a one-sided differencing approach as upstream or downstream values outside the computational

domain are not known. This default procedure on COMSOL can introduce significant errors at the left and right boundary points if the issue is not properly addressed.

The above issue of evaluation of $\vec{\tau}_2^{pi}$ was addressed here by using available values of $\vec{\tau}_2^{p}$ (from analytical adiabatic solution in Appendix A2) for $x^p = -x^{p*}$. For $x^p = L_{comp}$, the values close to $x^p \cong L_{comp}$ (for computations over $x^p \leq L < L_{comp}$) were used from their stored estimates for $x^p \cong L_{comp}$. These stored estimates were obtained from an earlier longer domain computations involving $L_{comp}|_{earlier} > L_{comp}$. For this reason, the solution reported here only cover the $-x^{p*} < x^p < L_{comp}$ domain. Note that the flow boiling solution of interest is typically only for uniform thermal boundary conditions (Fig 2.2) over $x^p > 0$.

4. Results and Discussions

4.1 Grid Size Restrictions

From the Discrete Fourier Transforms (DFT) of key x-dependent functions of $\delta(x)$, $\bar{u}(x)$, $\bar{v}(x)$, τ^{i}_{2x}, τ^{i}_{2y}, etc.; their dominant spatial frequencies are ascertained. Then the smallest spatial length λ_x that needs to be resolved is ascertained. Then the spatial discretization Δx_{f-g} in step (vi) is so chosen that it not only satisfies all interfacial conditions but that it can also resolve the flow-physics constraints on the resolvable length scales of interest (including the largest length $L = L_{comp}$). That is, the Nyquist criteria [37] is satisfied by imposing a more conservative (than Nyquist criteria: $\lambda_x/2 < \Delta x_{f-g} < L$) restriction of $\lambda_x/6 < \Delta x_{f-g} < L/2$.

It should be noted that, after ensuring mesh-type independence (quadrilateral v/s triangular meshes) for steady solutions, only triangular meshes were chosen for superior performance in steady CFD simulations used for the 2-D liquid and the vapor domains (for discretization of interface conditions used as interface boundary conditions in COMSOL solvers, the choice was $\Delta x_{f-g} < \Delta x^{*}_{f-g}$. Here Δx^{*}_{f-g} values were such that, post-convergence, both the more conservative Nyquist criteria and discretized interface-conditions were satisfied. Part of the vapor domain in Fig. 2.1b shows the choice of triangular elements. In both the phases, the actual mesh is non-uniform as COMSOL's mesh generation function makes them more refined near the interface and the walls. This mesh-generation function is considered "fixed" for the reported simulations and mesh-size calculations. It is seen that, typically, the accuracy of the simulation is essentially a function of smallest mesh size in

any particular domain. Thus the smallest mesh size for liquid and vapor domains – denoted as Δs_L and Δs_V respectively – are considered to be representative of average mesh sizes for the respective domains.

Besides the fluid-physics based constraints on $\Delta x < \Delta x^*_{f-g}$, there are additional constraints that arise from the algorithm. These are $\Delta s_L < \Delta s^*_L$ and $\Delta s_V < \Delta s^*_V$. Here, Δs^*_L and Δs^*_V represent the liquid and vapor domain mesh-size values below which mesh-size independent solutions are obtained - such as those shown in Fig. 3.1 (also see [30, 38]).

It is found that, typically, Δx^*_{f-g} needed for resolving fluid physics and accurate satisfaction of all interface conditions is much coarser than the thin liquid film domain mesh sizes (i.e., $\Delta x^*_{f-g} >> \Delta s^*_L$) required for accurate liquid domain COMSOL solution (i.e. $\Delta s_L < \Delta s^*_L$, where Δs^*_L is ascertained as [30]). This relative coarseness of Δx^*_{f-g} allows CFD predicted x-variations (on Δs^*_L scale) of interfacial functions such as: $\delta(x), \bar{u}(x), \bar{v}(x), \tau^i_{2x}(x), \tau^i_{2y}(x)$ etc., to be "smoothed" and then re-mapped onto the desired $x_i = i.(\Delta x_{f\text{-}g})$ grid (also described in detail in [40])

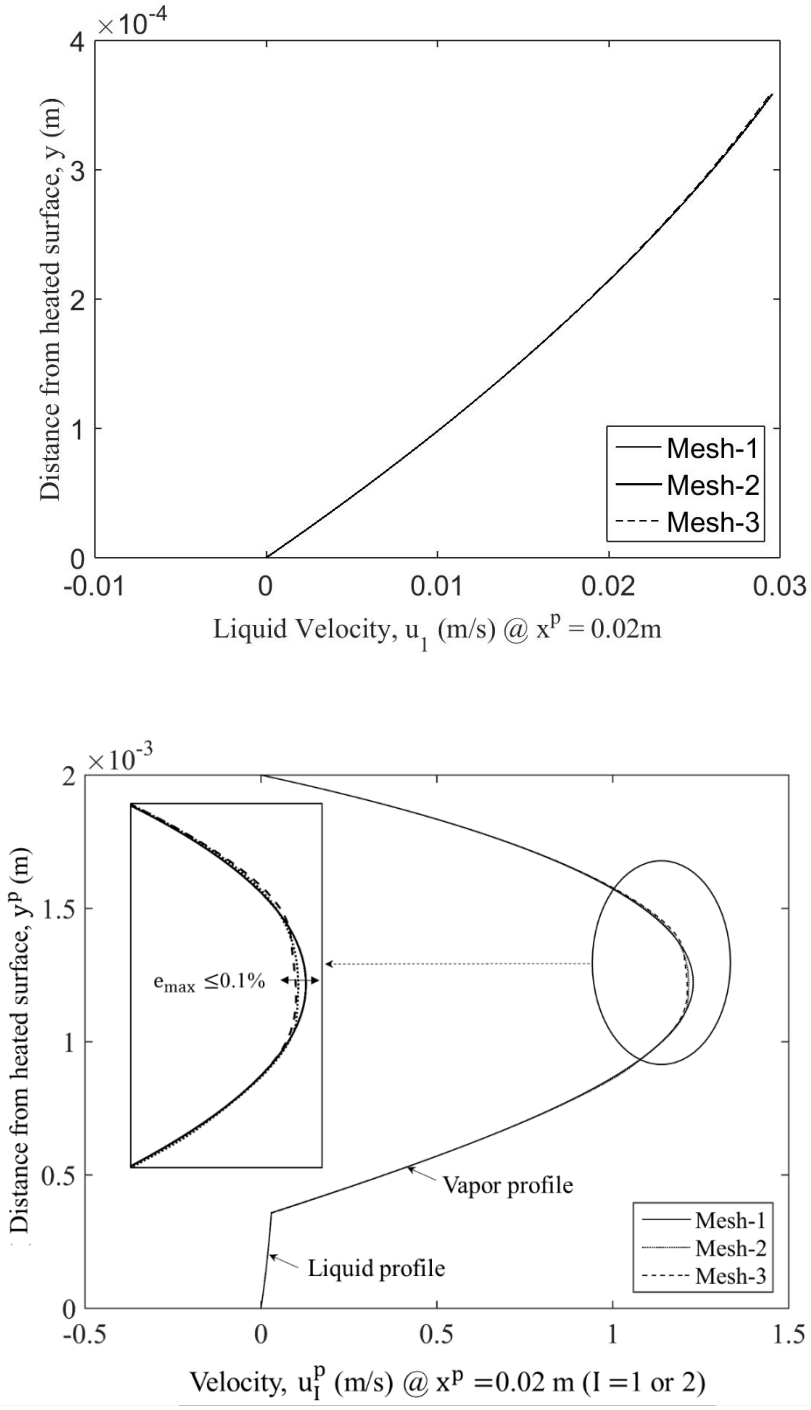

Fig 4.1: *The mesh comparison for:* ***(a)*** *a representative liquid domain solution and* ***(b)*** *a representative vapor domain solution. The "order of convergence" study, not reported here, yields results similar to what has been reported in [30, 38] (Run parameters: Fluid – FC72, U – 1 m/s, p_0 = 105.1 kPa, ΔT = 10°C, h = 2 mm).*

It can be noted from the Figs. 4.1 a & b, that $\Delta s_L^* > \Delta s_{L1}$ and $\Delta s_{v2} > \Delta s_V^* > \Delta s_{v1}$. Table 4.1 shows the representative mesh sizes for the three different meshes whose results are plotted in Fig. 4.1.

***Table 4.1**: Table shows representative mesh sizes for different meshes*

Mesh	Representative Liquid Domain Mesh sizes	Representative Vapor Domain Mesh sizes
Mesh-1	$\Delta s_{L1}=5.864\text{x}10^{-10}$	$\Delta s_{v1}=1.064\text{x}10^{-8}$
Mesh-2	$\Delta s_{L2}=7.02\text{x}10^{-10}$	$\Delta s_{v2}=1.069\text{x}10^{-9}$
Mesh-3	$\Delta s_{L3}=5.57\text{x}10^{-12}$	$\Delta s_{v3}=1.07\text{x}10^{-10}$

Furthermore, Table 4.2 shows satisfaction of all the interface conditions at discretized x-locations.

Table 4.2: *Table shows representative satisfaction of interface conditions for different locations along the length of the channel*

Location	Interfacial Mass Flux				Continuity of Tangential Velocities			Normal Component of Momentum Balance			Interfacial Temperatures				Tangential Component of Momentum Balance		
x	$\dot{m}_{VK}$	$\dot{m}_{LK}$	$\dot{m}_{Energy}$	Max Diff (%)	u_1^i	u_2^i+...	Diff (%)	p_1^i	p_2^i+...	Diff (%)	T_1^i	T_2^i	T_{sat}	Diff %	τ_1^i	τ_2^i+..	Diff %
m	kg/m²s	kg/m²s	kg/m²s		m/s	m/s		Pa	Pa		K	K	K		N/m²	N/m²	
0.0205	-0.0242	-0.0242	-0.0242	0	0.0293	0.0293	0	-4.47	-4.47	0	331.15	331.15	331.15	0	0.0271	0.0271	0
0.0705	-0.0264	-0.0264	-0.0264	0	0.0263	0.0267	0	-7.903	-7.903	1.2E-5	331.15	331.15	331.15	0	0.0265	0.0265	0
0.1102	-0.0288	-0.0288	-0.0288	0	0.0239	0.0242	1.2	-10.77	-10.77	0	331.15	331.15	331.15	0	0.0263	0.0263	0
0.1512	-0.0328	-0.0328	-0.0328	0	0.0205	0.0208	1.4	-13.874	-13.874	0	331.15	331.15	331.15	0	0.0258	0.0258	0
0.1909	-0.042	-0.042	-0.0417	0.7	0.0157	0.0156	0.6	-17.093	-17.092	1.2E-5	331.15	331.15	331.15	0	0.0246	0.0246	0

4.2 Basic Flow Features of Suppressed Nucleation Annular Boiling

The steady flow simulations yield elucidating information on two dimensional spatial variations of key 2-D flow variables of interest (I = 1 or 2), viz. velocity components (u_I, v_I), temperatures (T_I), pressures (p_I) etc. They also yield one dimensional spatial variations of key flow variables such as: film thickness $\Delta(x)$, x-component of interfacial velocity $u_1^i(x)$, characteristic speed $\bar{u}(x)$ associated with interfacial wave-propagation resulting from initial disturbances of infinitesimal amplitude, interfacial shear $\tau^{int}(x) \equiv (\tau_{2x}^i + \Delta'(x)\tau_{2y}^i)/\sqrt{1+\Delta_x^2}$, interfacial mass flux $\dot{m}^p(x^p)$, wall heat flux $q''_w(x)$, local values of heat transfer coefficient $h_x \equiv q''_w(x)/\left[T_w(x) - T_{sat}(p_0)\right]$, Nusselt number $Nu_x \equiv h_x.h/k_1$, and quality $X(x^p)$. The results also yield interfacial mechanical energy transfer terms $\dot{W}_{Mech}^{int}(x^p)$, identify the most significant term, and that term's relationship to other mechanical energy transfer term present in the interior of the flow field (see [38]). However, the heat transfer coefficient, Nusselt number, and mechanical energy transfer terms are not reported in the current thesis and will be reported later in [32].

For a representative horizontal ($\alpha = 0$) flow situation in Fig. 2.1a (also see Fig. 2.3), and under a steady "heating method" of the type defined in Fig. 2.2a (with $x^{p*} = -0.03$ m and $x^{p**} = -0.05$ m), the steady solution has been obtained by the algorithm proposed in section 3 and the plots for: film thickness $\Delta(x)$, versus x, cross-sectional profiles of $u_I(x^*,y)$, $v_I(x^*,y)$, $T_I(x^*,y)$ and $p_I(x^*,y)$ (for I = 1 & 2) versus y for a representative $x = x^*$ are respectively shown in Figs. 4.1 a-e. In Fig. 4.1, $x \geq 0$ with x = 0 as in Fig. 2.2a.

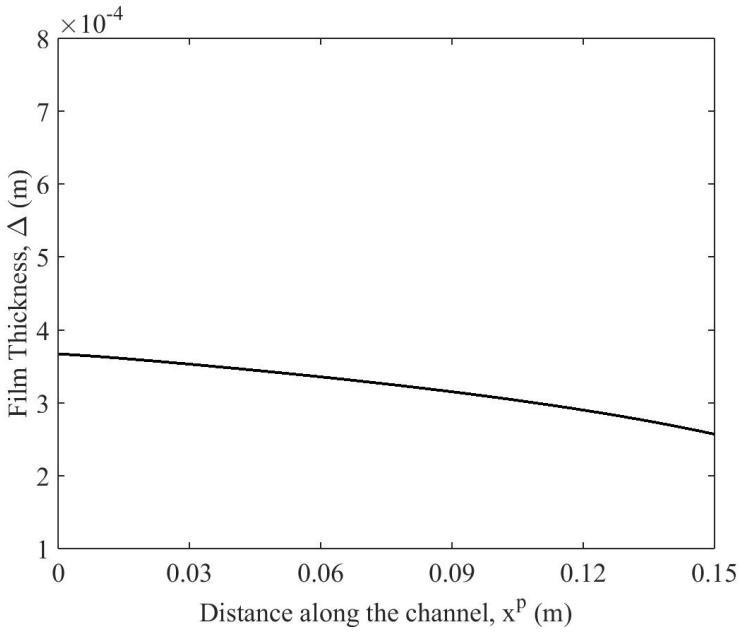
×10^-4
8
7
6
5
4
3
2
1
Film Thickness, Δ (m)
0
0.03
0.06
0.09
0.12
0.15
Distance along the channel, x^p (m)

(a)

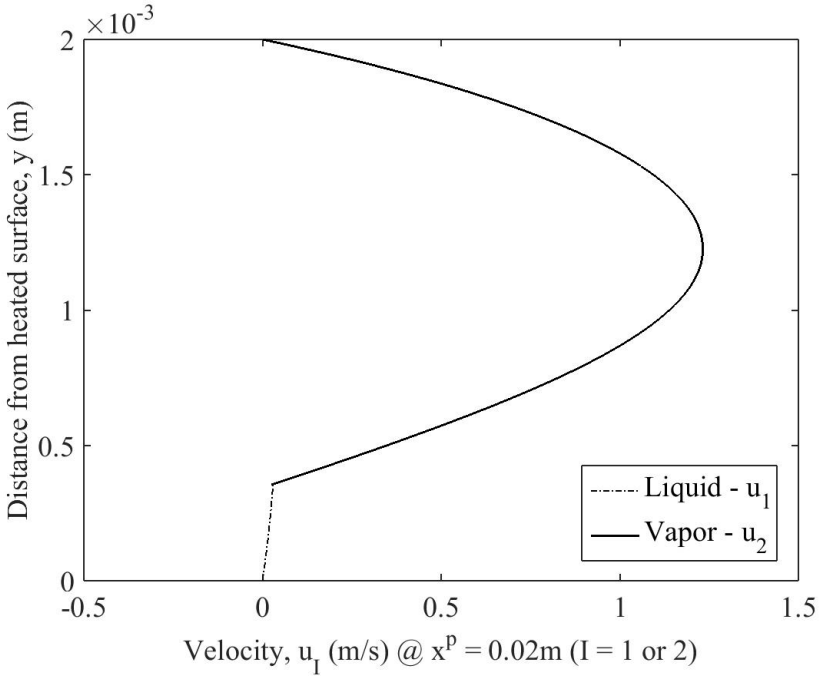
×10^-3
2
1.5
1
0.5
0
Distance from heated surface, y (m)
-0.5
0
0.5
1
1.5
Velocity, u_I (m/s) @ x^p = 0.02m (I = 1 or 2)
Liquid - u_1
Vapor - u_2

(b)

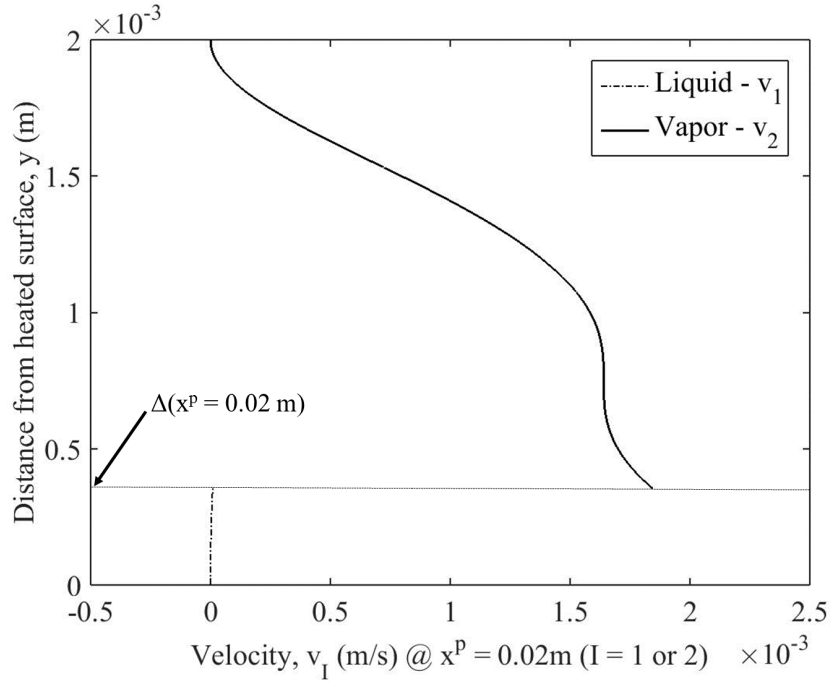
×10^-3
2
1.5
1
0.5
0
Distance from heated surface, y (m)
Liquid - v1
Vapor - v2
Δ(x^p = 0.02 m)
-0.5
0
0.5
1
1.5
2
2.5
Velocity, v_I (m/s) @ x^p = 0.02m (I = 1 or 2)
×10^-3

(c)

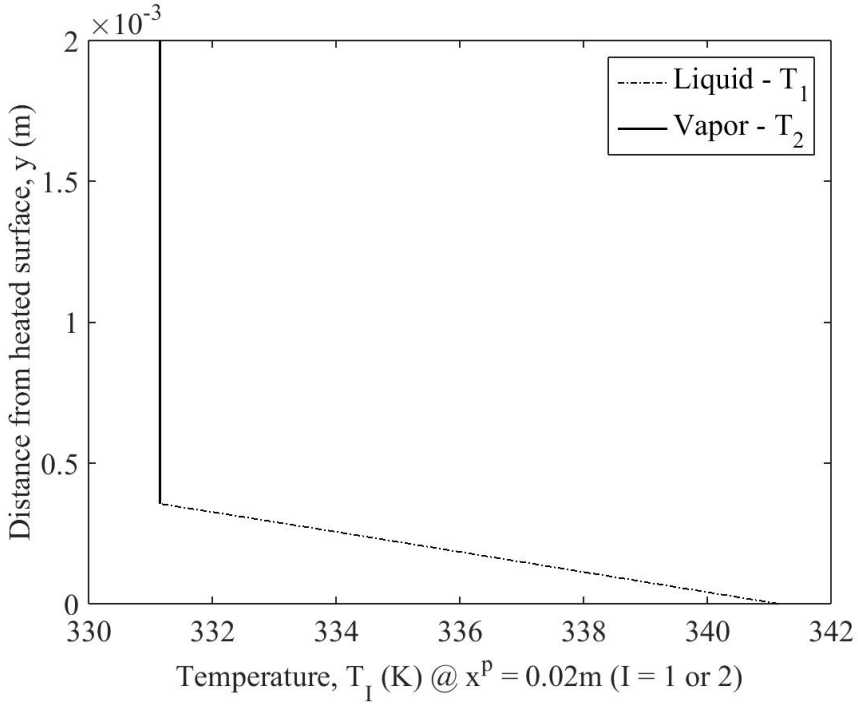
×10^-3
2
1.5
1
0.5
0
Distance from heated surface, y (m)
Liquid - T1
Vapor - T2
330
332
334
336
338
340
342
Temperature, T_I (K) @ x^p = 0.02m (I = 1 or 2)

(d)

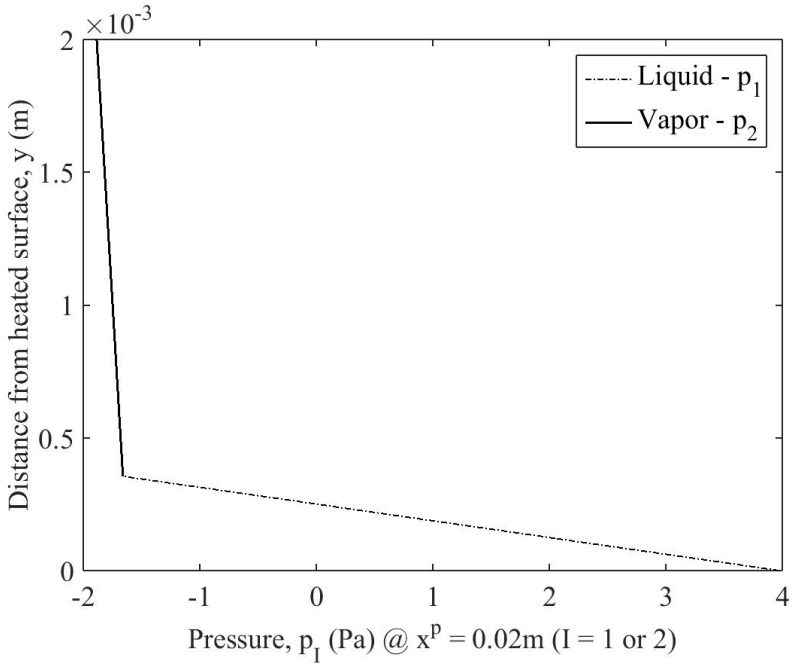
×10^-3
2
1.5
1
0.5
0
Distance from heated surface, y (m)
Liquid - p1
Vapor - p2
-2
-1
0
1
2
3
4
Pressure, pI (Pa) @ xp = 0.02m (I = 1 or 2)

(e)

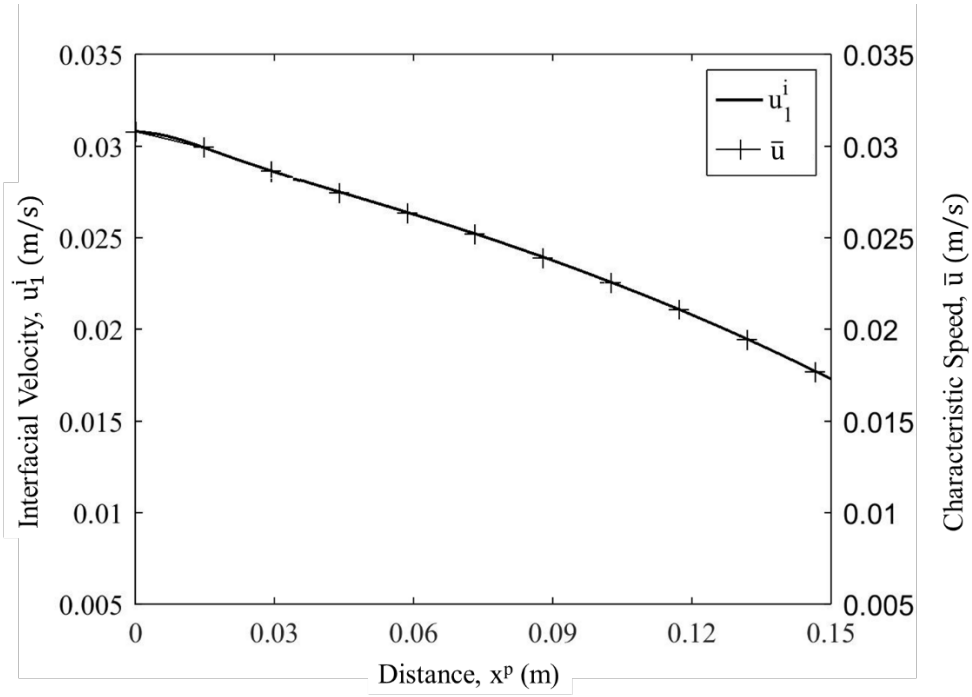
0.035
0.03
0.025
0.02
0.015
0.01
0.005
Interfacial Velocity, u1i (m/s)
Characteristic Speed, ū (m/s)
u1i
ū
0
0.03
0.06
0.09
0.12
0.15
Distance, xp (m)

(f)

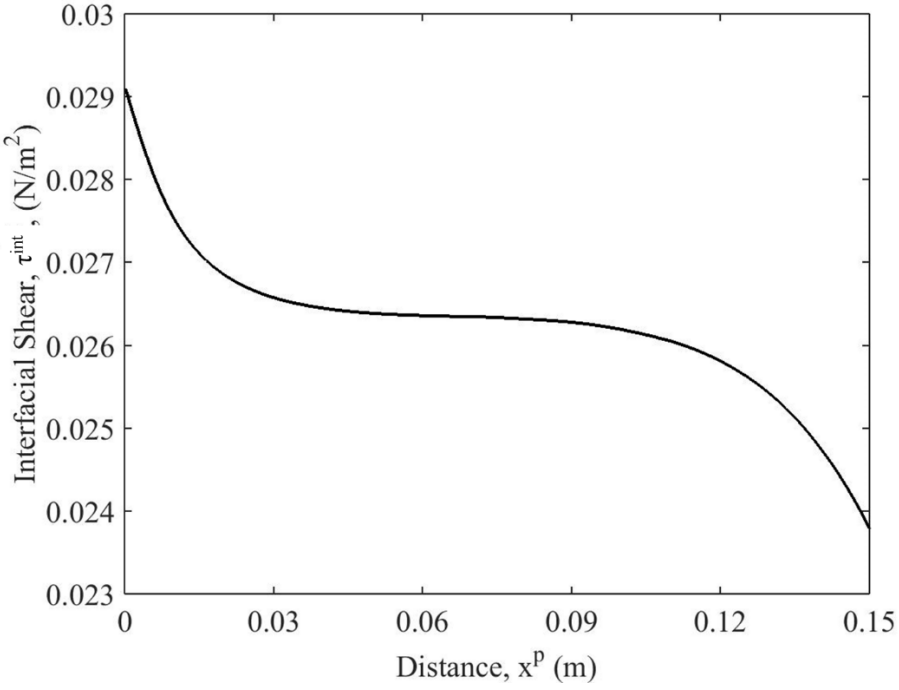

(g)

Fig. 4.2: (a) *Plot of a steady film thickness profile for a horizontal case involving presence of transverse gravity. Cross-sectional profile plots at x^p = 0.02 m are shown for:* ***(b)*** *x-component of velocity u_l,* ***(c)*** *y-component of velocity v_l, and* ***(d)*** *Temperature T_l, and* ***(e)*** *pressure p_l. The x-variation of 1-D flow variables:* ***(f)*** $\overline{u}(x^p)$ *and* $u_1^i(x^p)$ *;* ***(g)*** $\tau^{int}(x^p)$ *; (Run parameters: Fluid – FC-72, U = 1 m/s, p_0 = 105.1 kPa, ΔT = 10°C, channel height = 2 mm, $G \equiv \rho_2 U$ = 13.98 kg/m^{2}s)*

It is important to note that, relative to h = 2 mm, liquid film thickness Δ in Fig. 4.1a is very small (order of (Δ/h) is 10^{-1}). Also, the already small order of magnitude (~10^{-2}) of x-component of liquid velocity $u_1(x,y)$ relative to max vapor speed of ~ 1m/s, see Fig. 4.1b, is much larger than the order of magnitude (~ 10^{-5} m/s) of y-component of liquid velocity $v_1(x,y)$ - which has magnitudes, shown in Fig 4.1c, that are not even noticeable related to the magnitude of $v_2(x,y)$. Evaporation at the interface is associated with large density reduction – so there is a large increase in y-component of vapor velocity $v_2(x,y)$ near the interface (this is, also ~ 10^{-3} m/s, as shown in Fig. 4.1c). The cross-sectional temperature

T_I (x*,y) variations are shown in Fig. 4.1d, pressure variation $p_I(x,y)$ in the vapor (I = 2) and liquid (I = 1) phases – as shown in Fig. 4.1e – is primarily hydrostatic (for $g_y = -g$).

For the flow-case in Figs. 4.1-4.2, the x-variations in key variables of interest, viz: $\dot{m}^p(x^p)$, $q''_w(x^p)$ are shown in Figs. 4.3 a & b.

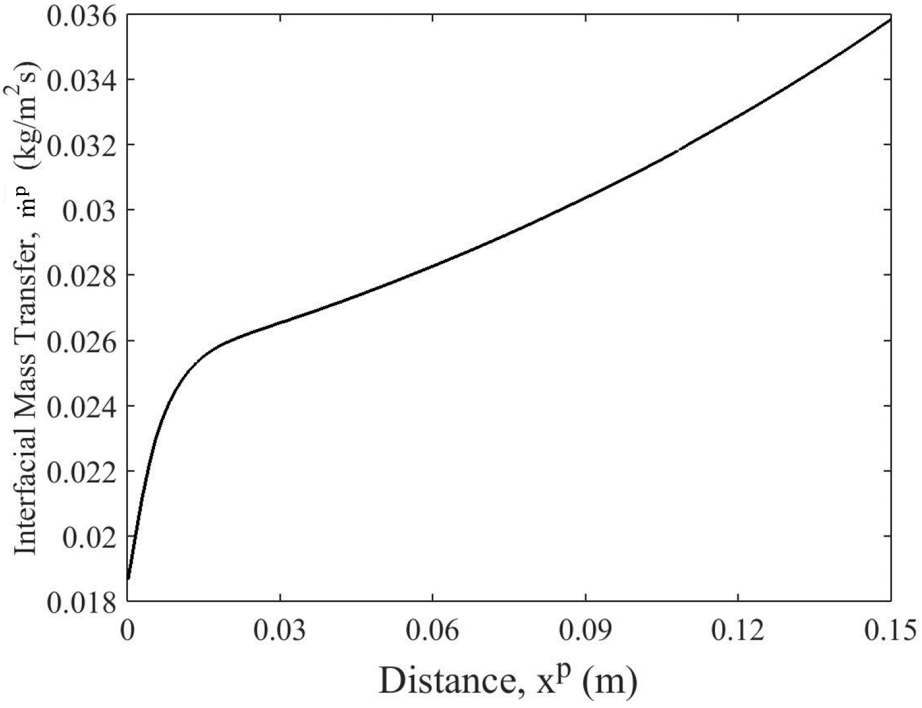

(a)

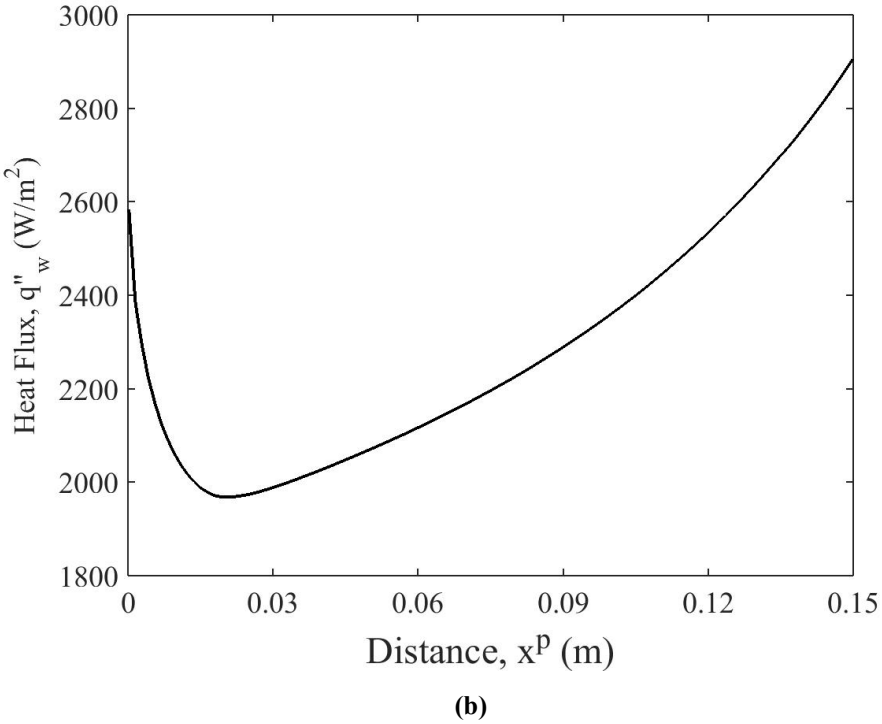

(b)

Fig. 4.3: *The x-variation of 1-D heat transfer variables for the flow in Fig. 4.2:* ***(a)*** $\dot{m}^p(x^p)$ ***(b)*** $q''_w(x)$ *(Run case: same as in Fig 4.2.)*

5. Conclusions

In summary, this paper accomplishes the following:

- It reports the development details of an accurate steady annular flow-boiling solution approach.

- The paper addressed some critical questions on how to obtain HTC correlations by detailed DNS CFD and proposed a correlations-based one-dimensional prediction approach for engineering design. This approach has been and is being used by the authors in the design of innovative flow-boilers [32].

- The solution technique, established here for the first time in this context of annular-boiling, establishes the expected equivalence of heat-flux and temperature controlled methods of heating.

- The paper discussed the role of various criteria for identifying "onset" of suppressed nucleation annular boiling as well as criteria for transition to relevant neighbouring non-annular (plug – slug, etc) regimes.

6. Forthcoming Results

This thesis enables the following type of results that are to be reported in [32]:

(i) Non-dimensional format of results that are correlated with flow-physics.

(ii) Descriptions showing equivalence of heat-flux and wall temperature prescriptions as thermal boundary conditions representing different "methods of heating".

(iii) Non-dimensional heat transfer correlations (i.e., for Nusselt Number) for prescribed wall temperature and wall heat-flux boundary conditions – allowing for entrance effects to the conditions prior to the test section inlet ($x^p < 0$).

(iv) Criteria estimating transitions between annular and non-annular (plug-slug regimes for cases of interest) flow regimes.

(v) Comparison of DNS-CFD results with predictions from relevant well known correlations for heat transfer coefficient and pressure drop.

REFERENCES

1. Kivisalu, M.T., P. Gorgitrattanagul, and A. Narain, *Results for high heat-flux flow realizations in innovative operations of milli-meter scale condensers and boilers.* International Journal of Heat and Mass Transfer, 2014. **75**(0): p. 381-398.

2. Ghiaasiaan, S.M., Two-phase flow, boiling, and condensation: in conventional and miniature systems. 2007: Cambridge University Press.

3. Carey, V.P., Liquid-vapor phase-change phenomena : an introduction to the thermophysics of vaporization and condensation processes in heat transfer equipment. 2nd ed. 2008, New York: Taylor and Francis. xxii, 742 p.

4. Bao, Z., D. Fletcher, and B. Haynes, *Flow boiling heat transfer of Freon R11 and HCFC123 in narrow passages.* International Journal of Heat and Mass Transfer, 2000. **43**(18): p. 3347-3358.

5. Saitoh, S., H. Daiguji, and E. Hihara, *Effect of tube diameter on boiling heat transfer of R-134a in horizontal small-diameter tubes.* International Journal of Heat and Mass Transfer, 2005. **48**(23-24): p. 4973-4984.

6. Consolini, L., Convective boiling heat transfer in a single micro-channel. 2008.

7. Greco, A., Convective boiling of pure and mixed refrigerants: An experimental study of the major parameters affecting heat transfer. International Journal of Heat and Mass Transfer, 2008. **51**(3-4): p. 896-909.

8. Qu, W. and I. Mudawar, *Flow boiling heat transfer in two-phase micro-channel heat sinks—II. Annular two-phase flow model.* International Journal of Heat and Mass Transfer, 2003. **46**(15): p. 2773-2784.

9. Kandlikar, S.G. and P. Balasubramanian, An Extension of the Flow Boiling Correlation to Transition, Laminar, and Deep Laminar Flows in Minichannels and Microchannels. Heat Transfer Engineering, 2004. **25**(3): p. 86-93.

10. Harirchian, T. and S.V. Garimella, *Flow regime-based modeling of heat transfer and pressure drop in microchannel flow boiling.* International Journal of Heat and Mass Transfer, 2012. **55**(4): p. 1246-1260.

11. Kim, S.M. and I. Mudawar, *Universal approach to predicting heat transfer coefficient for condensing mini/micro-channel flow.* International Journal of Heat and Mass Transfer, 2013. **56**(1-2): p. 238-250.

12. Mukherjee, A. and V.K. Dhir, *Study of lateral merger of vapor during nucleate pool boiling.* Journal of Heat Transfer, 2004. **126**(6): p. 1023-1039.

13. Son, G. and V.K. Dhir, *A Level Set Method for Analysis of Film Boiling on an Immersed Solid Surface.* Numerical Heat Transfer, Part B: Fundamentals, 2007. **52**(2): p. 153-177.

14. Kunkelmann, C. and P. Stephan, *CFD Simulation of Boiling Flows Using the Volume-of-Fluid Method within OpenFOAM.* Numerical Heat Transfer, Part A: Applications, 2009. **56**(8): p. 631-646.

15. Sun, D.L. and W.Q. Tao, *A coupled volume-of-fluid and level set (VOSET) method for computing incompressible two-phase flows.* International Journal of Heat and Mass Transfer, 2010. **53**(4): p. 645-655.

16. Ling, K., Z.-Y. Li, and W.-Q. Tao, *A Direct Numerical Simulation for Nucleate Boiling by the VOSET Method.* Numerical Heat Transfer, Part A: Applications, 2014. **65**(10): p. 949-971.

17. Moriyama, K., A. Inoue, and H. Ohira, The thermohydraulic characteristics of two-phase flow in extremely narrow channels (the frictional pressure drop and heat transfer of boiling two-phase flow, analytical model). Heat transfer. Japanese research, 1992. **21**(8): p. 838-856.

18. Jacobi, A.M. and J.R. Thome, *Heat Transfer Model for Evaporation of Elongated Bubble Flows in Microchannels.* Journal of Heat Transfer, 2002. **124**(6): p. 1131.

19. Thome, J.R., V. Dupont, and A.M. Jacobi, *Heat transfer model for evaporation in microchannels. Part I: presentation of the model.* International Journal of Heat and Mass Transfer, 2004. **47**(14-16): p. 3375-3385.

20. Das, A.K., P.K. Das, and P. Saha, *Heat transfer during pool boiling based on evaporation from micro and macrolayer.* International Journal of Heat and Mass Transfer, 2006. **49**(19-20): p. 3487-3499.

21. LaClair, T.J. and I. Mudawar, Theoretical model for fast bubble growth in small channels with reference to startup of capillary pumped loops used in spacecraft thermal management systems. International Journal of Heat and Mass Transfer, 2009. **52**(3-4): p. 716-723.

22. Na, Y.W. and J. Chung, *Two-phase annular flow and evaporative heat transfer in a microchannel.* International Journal of Heat and Fluid Flow, 2011. **32**(2): p. 440-450.

23. Kivisalu, M.T., Experimental Investigation of Internal Condensing Flows, Their Sensitivity to Pressure Fluctuations and Heat Transfer Enhancements, in Mechanical Engineering. 2015, Michigan Technological University.

24. Chun, K.R. and R.A. Seban, *Heat Transfer to Evaporating Liquid Films.* Journal of Heat Transfer, 1971. **93**(4): p. 391-396.

25. Ueda, T., M. Inoue, and S. Nagatome, *Critical heat flux and droplet entrainment rate in boiling of falling liquid films.* International Journal of Heat and Mass Transfer, 1981. **24**(7): p. 1257-1266.

26. Mudawwar, I.A. and M.A. El-Masri, *Momentum and heat transfer across freely-falling turbulent liquid films.* International Journal of Multiphase Flow, 1986. **12**(5): p. 771-790.

27. Marsh, W.J. and I. Mudawar, *Predicting the onset of nucleate boiling in wavy free-falling turbulent liquid films.* International Journal of Heat and Mass Transfer, 1989. **32**(2): p. 361-378.

28. Narain, A., et al., Fundamental assessments and new enabling proposals for heat transfer correlations and flow regime maps for shear driven condensers in the annular/stratified regime. Journal of Thermal Engineering, 2015. **1**(4): p. 307-321.

29. Naik, R. and A. Narain, Steady and unsteady simulations for annular internal condensing flows, part II: Instability and flow regime transitions. Numerical Heat Transfer, Part B: Fundamentals, 2016: p. 1-16.

30. Naik, R., A. Narain, and S. Mitra, Steady and unsteady simulations for annular internal condensing flows, part I: Algorithm and its accuracy. Numerical Heat Transfer, Part B: Fundamentals, 2016: p. 1-22.

31. Thome, J.R. and J.E. Hajal, *Two-phase flow pattern map for evaporation in horizontal tubes: latest version.* Heat Transfer Engineering, 2003. **24**(6): p. 3-10.

32. Ranga Prasad, H., Assessment of Annular Flow Boiling in the Context of CFD Simulations, Experiments and Existing Correlations. 2017, Michigan Technological University.

33. Ross, H. and R. Radermacher, *Suppression of nucleate boiling of pure and mixed refrigerants in turbulent annular flow.* International journal of multiphase flow, 1987. **13**(6): p. 759-772.

34. Engineering Equatiopn Solver (EES). 2014. **Version 9.689**.

35. Delhaye, J.M., Jump Conditions and Entropy Sources in Two-phase Systems; Local Instant Formulation. International Journal of Multiphase Flow, 1974. **1**: p. 395-409.

36. Narain, A., et al., Direct computational simulations for internal condensing flows and results on attainability/stability of steady solutions, their intrinsic waviness, and their noise sensitivity. Journal of Applied Mechanics, 2004. **71**(1): p. 69-88.

37. *The MathWorks Inc.,.* MATLAB documentation., 2014.

38. Naik, R.R., Development of unsteady two-dimensional computational simulation tools for annular internal condensing flows--and their use for results on heat-transfer rates, flow physics, flow stability, and flow sensitivity. 2015, MICHIGAN TECHNOLOGICAL UNIVERSITY.

39. Zivi, S., *Estimation of Steady-State Void Fraction by Means of Principle of Minimum Energy Production.* ASME Journal of Heat Transfer, 1964. 86(2), p. 247-252.

40. Hrishikesh, P., et al., Shear driven suppressed Nucleation Annular Flow-boiling in Millimeter-scale channels: Direct Numerical Simulations and Proposed Heat Transfer Correlations. *Submitted to*: International Journal of Transport Phenomena, 2016.

APPENDICES

APPENDIX A1

The surface velocity $\vec{\mathbf{v}}_s$ of a point on the interface ($\Phi = 0$) at time t is associated with this point's movement to a new mapped position on the interface at time $t + \Delta t$. All such mappings must be such that the normal component of this $\vec{\mathbf{v}}_s$ is given by:

$$\vec{\mathbf{v}}_s.\hat{\mathbf{n}} = -\left(\partial\Phi/\partial t\right)\Big/|\,\vec{\nabla}\Phi\,| \tag{A1.1}$$

The tangential component of the vapor and the liquid velocities at the interface must be continuous, i.e.

$$\vec{\mathbf{v}}_1^{\,pi}.\hat{\mathbf{t}} = \vec{\mathbf{v}}_2^{\,pi}.\hat{\mathbf{t}} \tag{A1.2}$$

Allowing for variations in the surface tension, σ, over the interface such that the vector $\vec{\nabla}_s\sigma$ is primarily in the tangent plane, the normal component of momentum balance at a point on the interface is given in ([28, 30]) and simplifies to:

$$p_1^i = p_2^i + \left(\dot{m}^p\right)^2\left(\frac{1}{\rho_2} - \frac{1}{\rho_1}\right) + \sigma\vec{\nabla}_s.\hat{\mathbf{n}} \tag{A1.3}$$

The tangential component of momentum balance at any point on the interface, which allows for surface variations in the surface tension σ, reduce to:

$$\mathbf{S}_1^i\hat{\mathbf{n}}.\hat{\mathbf{t}} = \mathbf{S}_2^i\hat{\mathbf{n}}.\hat{\mathbf{t}} + \vec{\nabla}_s\sigma.\hat{\mathbf{t}} \tag{A1.4}$$

For the phase-change flow problems considered here, interfacial temperature variations are

negligible and there are no interfacial impurities. Hence the Marangoni term $\vec{\nabla}_s\sigma.\hat{\mathbf{t}}$ contributions can be ignored relative to the interfacial shear driven motion.

The mass-flux $\dot{m}^p$ is denoted, separately as $\dot{m}^p_{VK}$ and $\dot{m}^p_{LK}$, to indicate independent kinematic restrictions imposed by interfacial values of vapor and liquid velocities. Thus, the definitions are:

$$\dot{m}^p_{VK} \equiv \rho_2\left(\vec{\mathbf{v}}_2^{\,pi} - \vec{\mathbf{v}}_s\right).\hat{\mathbf{n}}\text{, and}$$
$$\dot{m}^p_{LK} \equiv \rho_1\left(\vec{\mathbf{v}}_1^{\,pi} - \vec{\mathbf{v}}_s\right).\hat{\mathbf{n}} \tag{A1.5}$$

The energy balance at a point on the interface, with energy fluxes being relative to moving interface, also imposes a restriction on the interfacial mass flux $\dot{m}^p_{Energy}$. Its approximation as discussed in [38] is:

$$\dot{m}^p_{Energy} \cong \frac{1}{h_{fg}}\left[-k_1\frac{\partial T_1}{\partial n^p}\bigg|^i + k_2\frac{\partial T_2}{\partial n^p}\bigg|^i\right] \tag{A1.6}$$

The assumption of equilibrium thermodynamics at the interface allows one to use thermodynamics tables [34] to estimate "h_{fg}" as $h_{fg} \cong h_{fg}\left(T_s\left(p_2^i\right)\right) \cong h_{fg}\left(T_s\left(p_0\right)\right)$.

However, when the liquid film in Fig. 2.1 becomes sufficiently thin with $\left|\Delta(x)\right| < \Delta_{cr}$, where Δ_{cr} could be as little as 10-15 nm or much larger, depending on the dynamics of the approach as well as the physical material constituting the fluid and the wettability of the boiling surface, disjoining pressure effects may be observed (see explanation in [38]).

Whenever the film thickness is sufficiently large (say >10μm) over most of the boiling flow regime, equilibrium thermodynamic assumption as well as negligible interfacial thermal resistance assumption typically hold (see [38]). For problems considered here, over $x^p>0$, equilibrium thermodynamic assumptions are good. This is because interfacial mass transfer rates, $\dot{m}^p$, is sufficiently small in non-dimensional terms i.e. $\dot{m} \equiv \dot{m}^p / \rho_1 U << 1$. Under these equilibrium conditions, for $x^p>0$, T_1^i and T_2^i respectively denote the liquid and vapor temperatures at the interface, the following scientific model of the equilibrium thermodynamics holds at the interface:

$$T_1^i \cong T_2^i \equiv T_{sat}(p_2^i) \tag{A1.7}$$

However for some "thin film" situations not considered here, Eq. (A1.7) assumption of negligible thermal resistance, i.e. $\Delta T^i / \Delta T << 1$ (where $\Delta T^i \equiv \left| T_1^i - T_2^i \right|$) assumption does not hold and $T_1^i \neq T_2^i$ can be modeled by one of the two approaches given in [38].

For such conditions, where liquid film is "thin" over most of the significant parts (as in pulsatile high heat flux cases in [1]) of the length of the channel in Fig. 2.1, one allows $T_1^i \neq T_2^i$ and introduces other modelling equations [38] and another restriction on the interfacial mass flux that requires $\dot{m}^p = \dot{m}^p_{kinetic}$, and $\dot{m}^p_{kinetic}$ is obtained through phase-change models based on Kinetic theory of gases [3] and is defined as:

$$\dot{m}^p_{kinetic} \cong \frac{2\sigma_c}{2-\sigma_c}\left[\frac{p_{sat}(T_2^i)}{(2\pi R T_2^i)^{\frac{1}{2}}} - \frac{p_{sat}(T_1^i)}{(2\pi R T_1^i)^{\frac{1}{2}}}\right] \tag{A1.8}$$

where σ_c is an "accommodation" coefficient ([2, 3]) and $R \equiv R_u / \overline{M}$ is a gas constant related to the universal gas constant, R_u, and fluid's molecular weight $\overline{M}$.

As discussed in [38], mass balance at any point on the interface requires a single-valued interfacial mass flux. That is, when $\Delta T^i / \Delta T << 1$, one only needs to satisfy

$$\dot{m}^p_{LK} = \dot{m}^p_{VK} = \dot{m}^p_{Energy} \equiv \dot{m}^p \tag{A1.9}$$

If $\Delta T^i / \Delta T$ is not insignificantly small, the model in Eq. (A1.9) is replaced by the new interfacial mass balance requirement:

$$\dot{m}^p_{LK} = \dot{m}^p_{VK} = \dot{m}^p_{Energy} = \dot{m}^p_{kinetic} \equiv \dot{m}^p \tag{A1.10}$$

APPENDIX A2

For the adiabatic zone $-x^{p^*} < x^p < -x^{p^{**}}$ in the thermal boundary conditions of Fig. 2.2, the annular liquid and vapor flows are of uniform temperatures $T_1(x,y) = T_2(x,y) = T_{sat}(p_0)$ and interfacial mass flux values are $\dot{m}^p \equiv 0$. Here p_0 is pressure at y = h, (at $x^p = -x^{p^*}$ in Fig. 2.2). This annular adiabatic laminar/laminar flow zone shown in Fig A2.1 below, easily yields an analytical solution of the type:

$$\vec{v}_1 = u_1(y)\hat{i}$$

$$\vec{v}_2 = u_2(y)\hat{i}, \text{ and} \qquad \text{(A2.1)}$$

$$\Delta(x) = \Delta_0$$

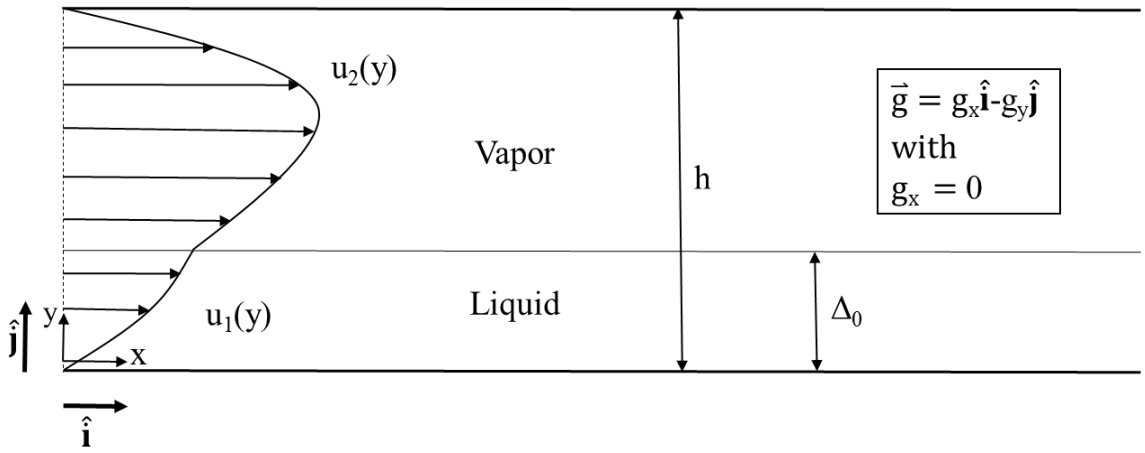

Fig A2.1: *Schematic of the adiabatic laminar/laminar flow zone corresponding to uniform liquid film thickness of Δ_0*

The x and y components of liquid (I = 1) and vapor (I = 2) momentum balance in Eq. (2.2) of section 2, when written in physical variables, yield solutions of the following structure:

$$p_1(x,y) = -\rho_1 g_y y + \lambda_1 x + \lambda_{11}$$

$$p_2(x,y) = -\rho_2 g_y y + \lambda_2 x + \lambda_{21}$$

$$u_1(y) = \frac{k_1}{2\mu_1} y^2 + k_{11} y + k_{12}$$

$$u_2(y) = \frac{k_2}{2\mu_2} y^2 + k_{21} y + k_{22} \qquad \text{(A2.1)}$$

$$\Delta(x) = \Delta_0$$

At the interface $y = \Delta_0 =$ constant, the continuity of tangential velocities (Eq. (2.3) with $\delta_x = 0$), tangential component of interfacial momentum balance (Eq. (2.5) with [t] = 0), and normal component of interfacial momentum balance (Eq. (2.4) with $\dot{m} = \delta_{xx} = 0$) come together to yield the following for the horizontal ($g_x = 0$) channel:

$$k_1 = k_2 = \lambda_2 = \lambda_1$$

$$k_{11} = \frac{\mu_2}{\mu_1} k_{21} \qquad \text{(A2.3)}$$

The non-slip condition at y = 0 and y = h yield

$$k_{12} = 0$$

$$k_{22} = -\left(\frac{k_2}{2\mu_2} h^2 + k_{21} h \right) \qquad \text{(A2.4)}$$

Denoting $p_2(-x^{p^*},h) = p_0$, the following is obtained for Eq. $(A2.1)_{1\text{-}2}$:

$$\lambda_2 = p_0 + \rho_2 g_y h$$

$$\lambda_{11} = \lambda_{22} + (\rho_1 - \rho_2) g_y \Delta_0 \tag{A2.5}$$

Next it can be found that the vapor flow rate per unit width, $\dot{M}_V$, in Fig. A2.1 is given by:

$$\dot{M}_V \equiv \int_{\Delta_0}^{h} \rho_2 u_2^p(y^p)dy^p \equiv \rho_2 k_2 \phi(\Delta_0, h) \tag{A2.6}$$

where, $$\phi(\Delta_0,h) = \left[\frac{1}{2\mu_2}\left(\frac{h^3-\Delta^3}{3}\right) + \psi(\Delta_0,h)\left(\frac{h^2-\Delta_0{}^2}{2}\right) - (h-\Delta_0)\left(\frac{h^2}{2\mu_2} + \psi(\Delta_0,h).h\right)\right]$$

and $$\psi(\Delta_0,h) = \frac{1}{2\mu_2}\frac{\left[-\Delta_0{}^2\left(1-\frac{\mu_1}{\mu_2}\right)+h^2\right]}{\left[\Delta_0\left(1-\frac{\mu_2}{\mu_1}\right)-h\right]}.$$

Further it can be found that,

$$\dot{M}_L \equiv \int_0^{\Delta_0} \rho_1 u_1^p(0,y^p)dy^p = \frac{\dot{M}_V}{\rho_2\phi(\Delta_0,h)}\left[\frac{\Delta_0{}^3}{6\mu_1} + \frac{\mu_2}{\mu_1}\frac{\Delta_0{}^2}{2}\psi(\Delta_0,h)\right] \tag{A2.7}$$

Using the notation,

$$\dot{M}_{in} \equiv \dot{M}_L + \dot{M}_V \text{ and,} \tag{A2.8}$$

$$X_{in} \equiv \dot{M}_V / \dot{M}_{in} \tag{A2.9}$$

it is easily shown that $\delta_0 \equiv \Delta_0 / h$ is the zero of the following non-dimensional equation:

$$\frac{1-X}{X}.\frac{\rho_2}{\rho_1} - \frac{1}{\hat{\phi}(\hat{\psi},\delta_0)}\left[\frac{\mu_2}{\mu_1}.\frac{1}{6}\delta_0^3 + \frac{\mu_2}{\mu_1}.\frac{\delta_0^2}{2}.\hat{\psi}\left(\delta_0, \frac{\mu_2}{\mu_1}\right)\right] = 0 \qquad \text{(A2.10)}$$

where, $\hat{\psi} \equiv \frac{1}{2}.\frac{\left[-\delta_0^2\left(1-\frac{\mu_2}{\mu_1}\right)+1\right]}{\left[\delta_0\left(1-\frac{\mu_2}{\mu_1}\right)-1\right]}$ and, $\hat{\phi} \equiv \left[\frac{1}{6}\left(1-\delta_0^3\right)+\hat{\psi}.\left(\frac{1-\delta_0^2}{2}\right)-\left(\frac{1-\delta_0}{2}+\hat{\psi}.\left(1-\delta_0\right)\right)\right]$

Clearly, the constant film thickness δ_0, a zero of Eq. (A2.10), is of the type:

$$\delta_0 = \delta_0\left(\frac{1-X}{X}.\frac{\rho_2}{\rho_1}, \frac{\mu_2}{\mu_1}\right) \qquad \text{(A2.11)}$$

Considering flow of refrigerants at an inlet pressure of p_0 = 1-2 bars, and annular zone qualities of $0.1 \le X \le 0.9$, it is found that for

$$0.003 \le \frac{\rho_2}{\rho_1} \le 0.016$$

$$0.02 \le \frac{\mu_2}{\mu_1} \le 0.036 \qquad \text{(A2.12)}$$

computationally obtained roots of Eq. (A2.10) for the parameters are correlated with mean error of 5.16% and maximum absolute error of 12.81% by the relationship:

$$\delta_0 = 0.4227\left(\frac{\mu_2}{\mu_1}\right)^{-0.2496}\left(\frac{1-X}{X}.\frac{\rho_2}{\rho_1}\right)^{0.3524} \tag{A2.13}$$

For parameters, covering both refrigerants and water at p_0 = 1-2 bars and $0.1 \le X \le 0.9$:

$$0.0006 \le \frac{\rho_2}{\rho_1} \le 0.016$$

$$0.02 \le \frac{\mu_2}{\mu_1} \le 0.055 \tag{A2.14}$$

the correlation:

$$\ln\delta_0 = -0.8147 - 0.1337\ln\left(\frac{\mu_2}{\mu_1}\right) + 0.29726\,n\left(\frac{1-X}{X}.\frac{\rho_2}{\rho_1}\right)$$

$$-0.0188\left[\ln\left(\frac{1-X}{X}.\frac{\rho_2}{\rho_1}\right)\right]^2 + 0.0371\ln\left(\frac{\mu_2}{\mu_1}\right).\ln\left(\frac{1-X}{X}.\frac{\rho_2}{\rho_1}\right) \tag{A2.15}$$

when compared with computed results has mean error of 0.35% and maximum absolute error of 1.87%.

The above results imply void fraction models of:

$$\varepsilon \equiv \frac{h-\Delta}{h} = 1-\delta_0 = 1-\left[0.4227\left(\frac{\mu_2}{\mu_1}\right)^{-0.2496}\left(\frac{1-X}{X}.\frac{\rho_2}{\rho_1}\right)^{0.3524}\right] \tag{A2.16}$$

and,

$$\varepsilon = 1-\delta_0 = 1-\exp(-0.8147-0.1337\ln\left(\frac{\mu_2}{\mu_1}\right)+0.2926\ln\left(\frac{1-X}{X}.\frac{\rho_2}{\rho_1}\right) \tag{A2.17}$$

$$-0.0188\left[\ln\left(\frac{1-X}{X}.\frac{\rho_2}{\rho_1}\right)\right]^2+0.0371.\ln\left(\frac{\mu_2}{\mu_1}\right).\ln\left(\frac{1-X}{X}.\frac{\rho_2}{\rho_1}\right))$$

A graphical comparison of Eq. (A2.16) and Eq. (A2.17) with Zivi correlation [39] given in Eq. (A2.18) is shown in Fig. A2.2 below. Comparisons with other popular correlation are to be reported in [32].

$$\varepsilon = \frac{1}{1+\frac{1-X}{X}\left(\frac{\rho_2}{\rho_1}\right)^{2/3}} \tag{A2.18}$$

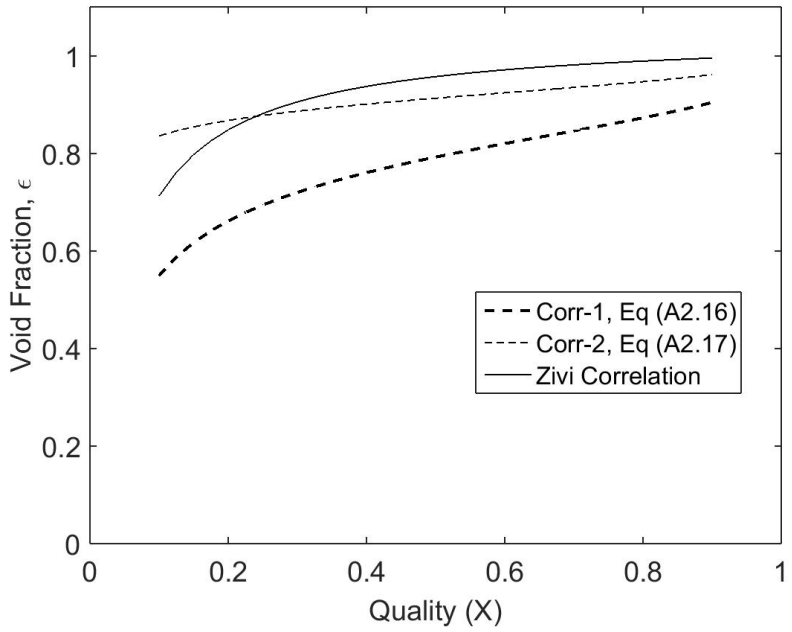

Fig A2.2: *Comparison of correlations with Zivi Correlation (Parameters:* (ρ_2/ρ_1) *= 0.0095,* (μ_2/μ_1) *= 0.024)*

With known, the velocity profiles in Eq. (A2.1) are obtained through:

$$k_1 = k_2 = \lambda_2 = \lambda_1 = \frac{\dot{M}_V}{\rho_2 \phi(\Delta_0, h)}$$

$$k_{21} = k_2 . \psi(\Delta_0, h)$$

$$k_{22} = -\left(\frac{k_2}{2\mu_2} h^2 + k_{21} h \right) \qquad \text{(A2.19)}$$

$$k_{11} = \frac{\mu_2}{\mu_1} k_{21}$$

The results in Eq. (A2.19) also give pressure fields (with p_0) and interfacial stress vector fields $\vec{\tau}_2^{pi}$ ($\equiv \vec{\tau}_{2x}^{i}\hat{\mathbf{i}} + \vec{\tau}_{2y}^{i}\hat{\mathbf{j}}$) through the relations:

$$p_1(x,y) = -\rho_1 g_y y + k_2 x + (\rho_1 - \rho_2) g_y \Delta_0 + p_0 + \rho_2 g_y \Delta_0$$

$$p_2(x,y) = \rho_2 g_y (\Delta_0 - y) + k_2 x + p_0$$

$$\tau_{2x}^{i} = -(k_2 \Delta_0 + \mu_2 k_{21}) \qquad \text{(A2.20)}$$

$$\tau_{2y}^{i} = p_0$$

APPENDIX A3

Figure 1.1 used with permission as documented in this copyright license.

ELSEVIER LICENSE
TERMS AND CONDITIONS

Jul 25, 2016

This Agreement between Sharayu S Bhasme ("You") and Elsevier ("Elsevier") consists of your license details and the terms and conditions provided by Elsevier and Copyright Clearance Center.

License Number	3915961007585
License date	Jul 25, 2016
Licensed Content Publisher	Elsevier
Licensed Content Publication	International Journal of Heat and Mass Transfer
Licensed Content Title	Results for high heat-flux flow realizations in innovative operations of milli-meter scale condensers and boilers
Licensed Content Author	M.T. Kivisalu,P. Gorgitrattanagul,A. Narain
Licensed Content Date	August 2014
Licensed Content Volume Number	75
Licensed Content Issue Number	n/a
Licensed Content Pages	18
Start Page	381
End Page	398
Type of Use	reuse in a thesis/dissertation
Portion	figures/tables/illustrations
Number of figures/tables/illustrations	1
Format	both print and electronic
Are you the author of this Elsevier article?	No
Will you be translating?	No
Order reference number	
Original figure numbers	Figure 2
Title of your thesis/dissertation	SHEAR DRIVEN SUPPRESSED NUCLEATION ANNULAR FLOW-BOILING IN MILLIMETER-SCALE CHANNELS: DIRECT NUMERICAL SIMULATIONS
Expected completion date	Aug 2016
Estimated size (number of pages)	70
Elsevier VAT number	GB 494 6272 12
Requestor Location	Sharayu S Bhasme 19472 Mayfield Avenue LIVONIA, MI 48152

United States
Attn: Sharayu S Bhasme

Total 0.00 USD

Terms and Conditions

INTRODUCTION

1. The publisher for this copyrighted material is Elsevier. By clicking "accept" in connection with completing this licensing transaction, you agree that the following terms and conditions apply to this transaction (along with the Billing and Payment terms and conditions established by Copyright Clearance Center, Inc. ("CCC"), at the time that you opened your Rightslink account and that are available at any time at http://myaccount.copyright.com).

GENERAL TERMS

2. Elsevier hereby grants you permission to reproduce the aforementioned material subject to the terms and conditions indicated.
3. Acknowledgement: If any part of the material to be used (for example, figures) has appeared in our publication with credit or acknowledgement to another source, permission must also be sought from that source. If such permission is not obtained then that material may not be included in your publication/copies. Suitable acknowledgement to the source must be made, either as a footnote or in a reference list at the end of your publication, as follows:
"Reprinted from Publication title, Vol /edition number, Author(s), Title of article / title of chapter, Pages No., Copyright (Year), with permission from Elsevier [OR APPLICABLE SOCIETY COPYRIGHT OWNER]." Also Lancet special credit - "Reprinted from The Lancet, Vol. number, Author(s), Title of article, Pages No., Copyright (Year), with permission from Elsevier."
4. Reproduction of this material is confined to the purpose and/or media for which permission is hereby given.
5. Altering/Modifying Material: Not Permitted. However figures and illustrations may be altered/adapted minimally to serve your work. Any other abbreviations, additions, deletions and/or any other alterations shall be made only with prior written authorization of Elsevier Ltd. (Please contact Elsevier at permissions@elsevier.com)
6. If the permission fee for the requested use of our material is waived in this instance, please be advised that your future requests for Elsevier materials may attract a fee.
7. Reservation of Rights: Publisher reserves all rights not specifically granted in the combination of (i) the license details provided by you and accepted in the course of this licensing transaction, (ii) these terms and conditions and (iii) CCC's Billing and Payment terms and conditions.
8. License Contingent Upon Payment: While you may exercise the rights licensed immediately upon issuance of the license at the end of the licensing process for the transaction, provided that you have disclosed complete and accurate details of your proposed use, no license is finally effective unless and until full payment is received from you (either by publisher or by CCC) as provided in CCC's Billing and Payment terms and conditions. If full payment is not received on a timely basis, then any license preliminarily granted shall be deemed automatically revoked and shall be void as if never granted. Further, in the event that you breach any of these terms and conditions or any of CCC's Billing and Payment terms and conditions, the license is automatically revoked and shall be void as if never granted. Use of materials as described in a revoked license, as well as any use of the materials beyond the scope of an unrevoked license, may constitute copyright infringement and publisher reserves the right to take any and all action to protect its copyright in the materials.
9. Warranties: Publisher makes no representations or warranties with respect to the licensed material.
10. Indemnity: You hereby indemnify and agree to hold harmless publisher and CCC, and their respective officers, directors, employees and agents, from and against any and all

claims arising out of your use of the licensed material other than as specifically authorized pursuant to this license.
11. No Transfer of License: This license is personal to you and may not be sublicensed, assigned, or transferred by you to any other person without publisher's written permission.
12. No Amendment Except in Writing: This license may not be amended except in a writing signed by both parties (or, in the case of publisher, by CCC on publisher's behalf).
13. Objection to Contrary Terms: Publisher hereby objects to any terms contained in any purchase order, acknowledgment, check endorsement or other writing prepared by you, which terms are inconsistent with these terms and conditions or CCC's Billing and Payment terms and conditions. These terms and conditions, together with CCC's Billing and Payment terms and conditions (which are incorporated herein), comprise the entire agreement between you and publisher (and CCC) concerning this licensing transaction. In the event of any conflict between your obligations established by these terms and conditions and those established by CCC's Billing and Payment terms and conditions, these terms and conditions shall control.
14. Revocation: Elsevier or Copyright Clearance Center may deny the permissions described in this License at their sole discretion, for any reason or no reason, with a full refund payable to you. Notice of such denial will be made using the contact information provided by you. Failure to receive such notice will not alter or invalidate the denial. In no event will Elsevier or Copyright Clearance Center be responsible or liable for any costs, expenses or damage incurred by you as a result of a denial of your permission request, other than a refund of the amount(s) paid by you to Elsevier and/or Copyright Clearance Center for denied permissions.

LIMITED LICENSE

The following terms and conditions apply only to specific license types:
15. **Translation**: This permission is granted for non-exclusive world **English** rights only unless your license was granted for translation rights. If you licensed translation rights you may only translate this content into the languages you requested. A professional translator must perform all translations and reproduce the content word for word preserving the integrity of the article.
16. **Posting licensed content on any Website**: The following terms and conditions apply as follows: Licensing material from an Elsevier journal: All content posted to the web site must maintain the copyright information line on the bottom of each image; A hyper-text must be included to the Homepage of the journal from which you are licensing at http://www.sciencedirect.com/science/journal/xxxxx or the Elsevier homepage for books at http://www.elsevier.com; Central Storage: This license does not include permission for a scanned version of the material to be stored in a central repository such as that provided by Heron/XanEdu.
Licensing material from an Elsevier book: A hyper-text link must be included to the Elsevier homepage at http://www.elsevier.com . All content posted to the web site must maintain the copyright information line on the bottom of each image.

Posting licensed content on Electronic reserve: In addition to the above the following clauses are applicable: The web site must be password-protected and made available only to bona fide students registered on a relevant course. This permission is granted for 1 year only. You may obtain a new license for future website posting.
17. **For journal authors:** the following clauses are applicable in addition to the above:
Preprints:
A preprint is an author's own write-up of research results and analysis, it has not been peer-reviewed, nor has it had any other value added to it by a publisher (such as formatting, copyright, technical enhancement etc.).
Authors can share their preprints anywhere at any time. Preprints should not be added to or enhanced in any way in order to appear more like, or to substitute for, the final versions of

articles however authors can update their preprints on arXiv or RePEc with their Accepted Author Manuscript (see below).
If accepted for publication, we encourage authors to link from the preprint to their formal publication via its DOI. Millions of researchers have access to the formal publications on ScienceDirect, and so links will help users to find, access, cite and use the best available version. Please note that Cell Press, The Lancet and some society-owned have different preprint policies. Information on these policies is available on the journal homepage.
Accepted Author Manuscripts: An accepted author manuscript is the manuscript of an article that has been accepted for publication and which typically includes author-incorporated changes suggested during submission, peer review and editor-author communications.
Authors can share their accepted author manuscript:

- immediately
  - via their non-commercial person homepage or blog
  - by updating a preprint in arXiv or RePEc with the accepted manuscript
  - via their research institute or institutional repository for internal institutional uses or as part of an invitation-only research collaboration work-group
  - directly by providing copies to their students or to research collaborators for their personal use
  - for private scholarly sharing as part of an invitation-only work group on commercial sites with which Elsevier has an agreement
- after the embargo period
  - via non-commercial hosting platforms such as their institutional repository
  - via commercial sites with which Elsevier has an agreement

In all cases accepted manuscripts should:

- link to the formal publication via its DOI
- bear a CC-BY-NC-ND license - this is easy to do
- if aggregated with other manuscripts, for example in a repository or other site, be shared in alignment with our hosting policy not be added to or enhanced in any way to appear more like, or to substitute for, the published journal article.

Published journal article (JPA): A published journal article (PJA) is the definitive final record of published research that appears or will appear in the journal and embodies all value-adding publishing activities including peer review co-ordination, copy-editing, formatting, (if relevant) pagination and online enrichment.
Policies for sharing publishing journal articles differ for subscription and gold open access articles:
Subscription Articles: If you are an author, please share a link to your article rather than the full-text. Millions of researchers have access to the formal publications on ScienceDirect, and so links will help your users to find, access, cite, and use the best available version.
Theses and dissertations which contain embedded PJAs as part of the formal submission can be posted publicly by the awarding institution with DOI links back to the formal publications on ScienceDirect.
If you are affiliated with a library that subscribes to ScienceDirect you have additional private sharing rights for others' research accessed under that agreement. This includes use for classroom teaching and internal training at the institution (including use in course packs and courseware programs), and inclusion of the article for grant funding purposes.
Gold Open Access Articles: May be shared according to the author-selected end-user license and should contain a CrossMark logo, the end user license, and a DOI link to the formal publication on ScienceDirect.
Please refer to Elsevier's posting policy for further information.

18. **For book authors** the following clauses are applicable in addition to the above: Authors are permitted to place a brief summary of their work online only. You are not allowed to download and post the published electronic version of your chapter, nor may you scan the printed edition to create an electronic version. **Posting to a repository:** Authors are permitted to post a summary of their chapter only in their institution's repository.
19. **Thesis/Dissertation**: If your license is for use in a thesis/dissertation your thesis may be submitted to your institution in either print or electronic form. Should your thesis be published commercially, please reapply for permission. These requirements include permission for the Library and Archives of Canada to supply single copies, on demand, of the complete thesis and include permission for Proquest/UMI to supply single copies, on demand, of the complete thesis. Should your thesis be published commercially, please reapply for permission. Theses and dissertations which contain embedded PJAs as part of the formal submission can be posted publicly by the awarding institution with DOI links back to the formal publications on ScienceDirect.

Elsevier Open Access Terms and Conditions
You can publish open access with Elsevier in hundreds of open access journals or in nearly 2000 established subscription journals that support open access publishing. Permitted third party re-use of these open access articles is defined by the author's choice of Creative Commons user license. See our open access license policy for more information.
Terms & Conditions applicable to all Open Access articles published with Elsevier:
Any reuse of the article must not represent the author as endorsing the adaptation of the article nor should the article be modified in such a way as to damage the author's honour or reputation. If any changes have been made, such changes must be clearly indicated.
The author(s) must be appropriately credited and we ask that you include the end user license and a DOI link to the formal publication on ScienceDirect.
If any part of the material to be used (for example, figures) has appeared in our publication with credit or acknowledgement to another source it is the responsibility of the user to ensure their reuse complies with the terms and conditions determined by the rights holder.
Additional Terms & Conditions applicable to each Creative Commons user license:
CC BY: The CC-BY license allows users to copy, to create extracts, abstracts and new works from the Article, to alter and revise the Article and to make commercial use of the Article (including reuse and/or resale of the Article by commercial entities), provided the user gives appropriate credit (with a link to the formal publication through the relevant DOI), provides a link to the license, indicates if changes were made and the licensor is not represented as endorsing the use made of the work. The full details of the license are available at http://creativecommons.org/licenses/by/4.0.
CC BY NC SA: The CC BY-NC-SA license allows users to copy, to create extracts, abstracts and new works from the Article, to alter and revise the Article, provided this is not done for commercial purposes, and that the user gives appropriate credit (with a link to the formal publication through the relevant DOI), provides a link to the license, indicates if changes were made and the licensor is not represented as endorsing the use made of the work. Further, any new works must be made available on the same conditions. The full details of the license are available at http://creativecommons.org/licenses/by-nc-sa/4.0.
CC BY NC ND: The CC BY-NC-ND license allows users to copy and distribute the Article, provided this is not done for commercial purposes and further does not permit distribution of the Article if it is changed or edited in any way, and provided the user gives appropriate credit (with a link to the formal publication through the relevant DOI), provides a link to the license, and that the licensor is not represented as endorsing the use made of the work. The full details of the license are available at http://creativecommons.org/licenses/by-nc-nd/4.0.
Any commercial reuse of Open Access articles published with a CC BY NC SA or CC BY NC ND license requires permission from Elsevier and will be subject to a fee.
Commercial reuse includes:

- Associating advertising with the full text of the Article
- Charging fees for document delivery or access
- Article aggregation
- Systematic distribution via e-mail lists or share buttons

Posting or linking by commercial companies for use by customers of those companies.

20. **Other Conditions**:

v1.8

Questions? customercare@copyright.com or +1-855-239-3415 (toll free in the US) or +1-978-646-2777.